nature aging

Article

https://doi.org/10.1038/s43587-025-00996-x

Effect of the mitophagy inducer urolithin A on age-related immune decline: a randomized, placebo-controlled trial

Received: 3 November 2024

Accepted: 25 September 2025

Published online: 31 October 2025

Check for updates

A list of authors and their affiliations appears at the end of the paper

Mitochondrial dysfunction and stem cell exhaustion contribute to age-related immune decline, yet clinical interventions targeting immune aging are lacking. Recently, we demonstrated that urolithin A (UA), a mitophagy inducer, expands T memory stem cells (T_{SCM}) and naive T cells in mice. In this randomized, double-blind, placebo-controlled trial, 50 healthy middle-aged adults received oral UA (1,000 mg day^{-1}) or placebo for 4 weeks; time points of analysis were baseline and day 28. Primary outcomes were phenotypical changes in peripheral $CD3^+$ T cell subsets and immune metabolic remodeling. UA expanded peripheral naive-like, less terminally exhausted $CD8^+$ cells (treatment difference 0.50 percentage points; 95% CI = 0.16 to 0.83; $P = 0.0437$) while also increasing $CD8^+$ fatty acid oxidation capacity (treatment difference = 14.72 percentage points; 95% confidence interval (CI) = 6.46 to 22.99; $P = 0.0061$). Secondary outcomes included changes in plasma cytokine levels (IL-6, TNF, IL-1β, IL-10), immune populations assessed via flow cytometry, immune cell function, and mitochondrial content. Analysis revealed augmented mitochondrial biogenesis in $CD8^+$ cells, increased peripheral $CD56^{dim}CD16^{bright}$ NK cells, and nonclassical $CD14^{lo}CD16^{hi}$ monocytes in UA-treated participants, as well as improved activation-elicited TNF secretion in T cells and bacterial uptake by monocytes. Exploratory single-cell RNA sequencing demonstrated UA-driven transcriptional shifts across immune populations, modulating pathways linked to inflammation and metabolism. These findings indicate that short-term UA supplementation modulates human immune cell composition and function, supporting its potential to counteract age-related immune decline and inflammaging. ClinicalTrials.gov registration number: NCT05735886.

The immune system responds to harmful stimuli such as infections and cellular damage[1], playing a critical role in regulating inflammatory signaling required to combat exogenous infections or elicit an initial antitumor response at the presence of malignancy[2,3]. A remarkable feature of the immune system is its capacity to form a long-term adaptive response enabling a rapid recall to future re-challenges termed immune memory[4], providing specific immunity that can span over decades[5]. Yet, this principally advantageous plasticity actively specializing the immune system throughout life comes at the cost of reduced responsiveness to novel antigens which is highlighted by attenuated responses to vaccines and increased vulnerability to novel infectious diseases[6,7]. Immune aging describes the global remodeling of the immune system that is characterized by reduced thymic output and an increase in memory populations with concomitant reduction in naive T cell populations[8,9]. These changes cumulate in a chronic low-grade inflammatory state termed inflammaging[10,11] that is characterized by increased

e-mail: greten@gsh.uni-frankfurt.de

concentrations of pro-inflammatory mediators favoring the development of heart disease and cancer[12,13].

The emerging field of immunometabolism has highlighted the critical role of metabolic dependencies of immune cells and their organelles in regulating immune fate and function[14]. Mitophagy is a selective form of autophagy aimed at degrading damaged and dysfunctional mitochondria, with impaired mitophagy capacities constituting a defining characteristic of a variety of chronic conditions[15]. Indeed, inhibition of autophagy and impaired mitochondrial function constitute two of the hallmarks of aging[16]. Mitochondrial quality control also critically affects immune fate and function, in turn affecting systemic inflammaging[17]. T cells with dysfunctional mitochondrial dynamics provoke systemic senescence via pathological cytokine secretion[18], thereby placing them at the center of age-associated multimorbidity. In cancer, exhausted tumor-infiltrating leukocytes accumulate dysfunctional mitochondria caused by impairment of mitophagy[19] and repression of peroxisome proliferator-activated receptor gamma coactivator 1-alpha (PGC-1α)-mediated mitochondrial biogenesis[20]. Improving mitochondrial quality control therefore possesses great hypothetical potential for improving immune function and positively influencing aging-associated diseases characterized by a dysfunctional immune response. Yet, interventions aimed at improving immune health are currently restricted to generalized lifestyle interventions such as physical exercise[21] or caloric restriction[22], as hypothetical therapeutic approaches exhibit long-term safety concerns[23].

Urolithin A (UA) is a postbiotic metabolite derived from ellagitannins, of which pomegranates constitute a rich source[24]. UA potently induces mitophagy in humans and rodents[25,26], whereas clinical trials have demonstrated improved physical performance upon UA supplementation[27,28]. We have recently shown that UA directly regulates $CD8^+$ (cluster of differentiation 8-positive) T cell fate, leading to the expansion of T memory stem cells (T_{SCM}) and naive-like T cells (T_N) with potent anti-tumor memory in mice via mitophagy-elicited activation of Wnt signaling and T cell factor 1 (TCF1) induction[29]. We found that exposure to UA confers a beneficial T cell state on human chimeric antigen receptor (CAR) T cells ex vivo[29]. Therefore, we hypothesized that oral UA supplementation could trigger a similar effect associated with improved immune function in humans.

Results

The present study was designed as a randomized, double-blind, placebo-controlled proof-of-concept trial to investigate the effect of short-term (4 weeks) UA supplementation on immune health and systemic inflammation in a study cohort of 50 healthy middle-aged adults (MitoImmune, NCT05735886). Primary end points were changes in T cell subpopulations, as well as changes in mitochondrial activity in $CD3^+$ T cells compared to placebo. A 1 month intervention period was chosen according to the average lifespan of human effector and memory T cell populations[30]. We screened $n = 79$ study participants out of whom 50 successfully met all screening inclusion and exclusion criteria (Fig. 1). Participants were deemed healthy by a study physician as determined by their medical history, anthropometric measurements, physical examination, vital signs, and laboratory parameters. Randomization was performed based on age, gender, and body mass index (BMI), and participants were allocated to the treatment groups 1:1. Therefore, baseline characteristics of participants were similar (Table 1). Overall, there were more female participants (60% female versus 40% male) who were equally distributed to both groups. Vital signs did not differ between both groups at baseline (Table 1). Also, baseline levels of metabolic markers, kidney function parameters, and liver enzymes did not differ between the two groups (Extended Data Table 1).

Biochemical safety analysis and adverse event recording

Previously, long-term UA oral administration over 4 months was found to be safe and well tolerated in a cohort of middle-aged adults[27]. In line with this, only a total of nine adverse events were recorded during the 28 day study period in both groups (Extended Data Table 2). Four were reported in the UA group, whereas five were reported in the placebo group. Most adverse events ($n = 6$) were upper respiratory tract infections, of which three ($n = 3$) constituted SARS-CoV2 infections. One participant in the placebo group ($n = 1$) discontinued intake upon a major depressive episode which was deemed unrelated to the intervention. By protocol, no participants were excluded from final analysis, and analysis was performed by the original assigned group.

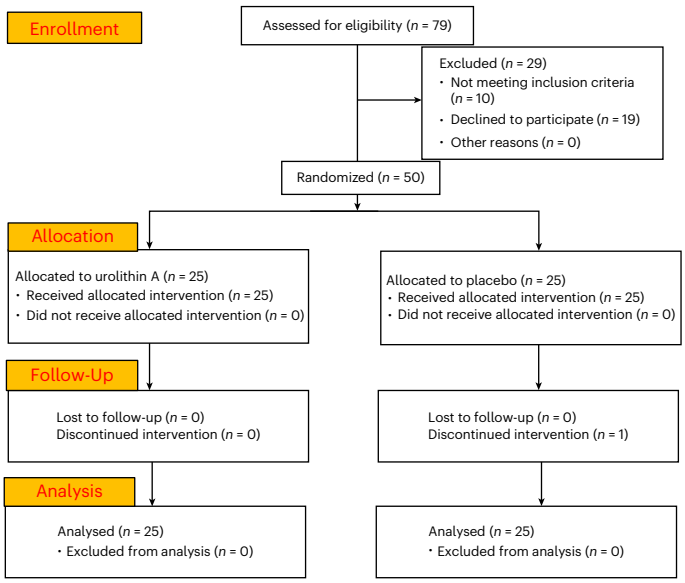

Fig. 1 | CONSORT diagram of participant inclusion. The MitoImmune trial was a single-center, randomized, double-blind, placebo-controlled, investigator-initiated interventional trial performed with healthy adults aged 45–70 years. Fifty participants ($n = 50$) met the inclusion and exclusion criteria and were subsequently included into the trial and then randomized to a daily intervention of single-dose (1,000 mg) UA or placebo based on age, gender, and BMI in a 1:1 ratio. The total study duration was 28 days. One participant did not complete the allocated trial product intake ($n = 1$ dropout) but provided samples for end point analysis. No participant was therefore excluded for the final analysis. Fourty-nine participants reported >90% intake compliance as assessed via questionaires and completed scheduled visits ($n = 49$).

Table 1 | Study participant demographics

	Urolithin A	Placebo	*P* value (significance)
Sex, female (%)	60	60	1.0 (NS)
Sex, male (%)	40	40	1.0 (NS)
Age (years) (mean±s.d.)	53.68±5.25	53.20±6.10	0.7669 (NS)
Weight (kg) (mean±s.d.)	74.58±15.45	76.12±14.89	0.7245 (NS)
BMI ($kg\,m^{-2}$) (<35 $kg\,m^{-2}$) (mean±s.d.)	25.33±3.59	25.91±4.50	0.6229 (NS)
Systolic blood pressure (mmHg) (mean±s.d.)	127.6±11.81	132.6±12.66	0.1843 (NS)
Diastolic blood pressure (mmHg) (mean±s.d.)	73.23±11.08	73.74±13.03	0.8880 (NS)
Heart rate (b.p.m.) (mean) (mean±s.d.)	66.90±6.72	70.79±7.19	0.0690 (NS)

Fifty participants ($n = 50$) that successfully met all inclusion and exclusion criteria were randomized to either UA or placebo. The two study groups were balanced on age, gender, BMI, and vital signs. Statistical analysis of baseline characteristics was performed via two-sided *t*-test.

https://doi.org/10.1038/s43587-025-00996-x

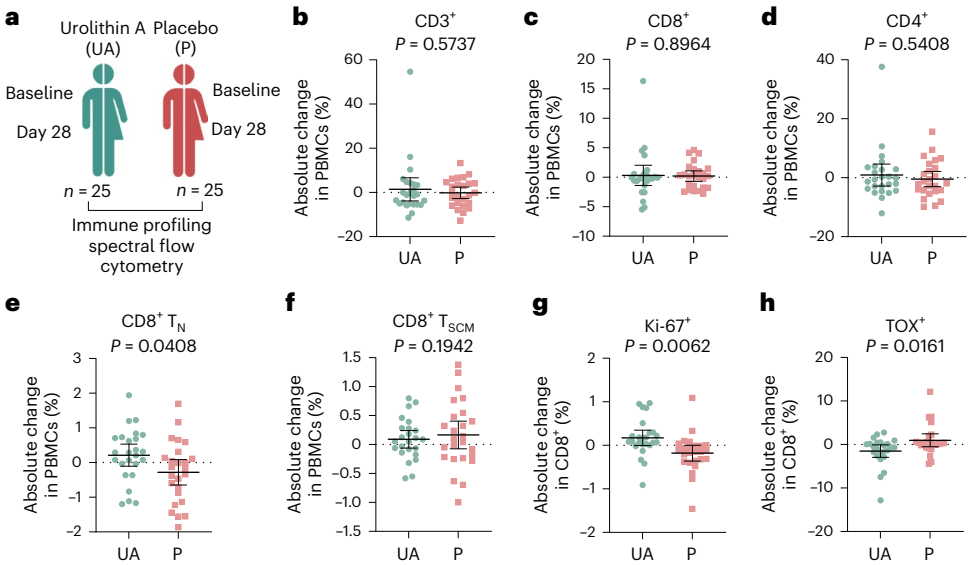

Fig. 2 | Primary end point—UA alters the CD8⁺ T cell phenotype. a, Experimental overview. PBMCs from the UA intervention cohort (UA) and placebo cohort (P) were subjected to spectral flow cytometry. Immune profiling was performed with matched samples from all three study visits. **b**–**d**, Changes in the T cell compartment as assessed by spectral flow cytometry. Changes of CD3⁺ αβ T cells (**b**), CD8⁺ T cells (**c**), and CD4⁺ cells (**d**) depicted as absolute change in percentage points of PBMCs are shown after 28 days of UA intake or placebo. Data are mean ± 95% confidence interval (CI), $n = 25$ per group. *P* values for treatment effects were calculated using a repeated measures mixed-effects model. **e**,**f**, Changes in CD8⁺ phenotype after 28 days. Absolute changes in percentage of naive CD8⁺ T cells (T_N; **e**) and CD8⁺ T_{SCM} (**f**) are shown. Data are mean ± 95% CI, $n = 25$ per group. *P* values for treatment effects were calculated using a repeated measures mixed-effects model. **g**,**h**, Absolute changes of Ki-67 (**g**) expression and TOX expression (**h**) within CD8⁺ cells after 28 days. Data are mean ± 95% CI, $n = 25$ per group. *P* values for treatment effects were calculated using a repeated measures mixed-effects model. All statistical tests were two-sided. No adjustment for multiple comparisons were made. Schematic in **a** created using BioRender.com.

No other differences in adverse events were reported between the two groups, confirming safety and tolerance of UA supplementation in aged adults without prior conditions. No significant changes were observed in kidney function parameters or liver enzymes after the 28 days of either UA or placebo (Extended Data Table 1). The intake of UA led to high plasma levels of parent UA and its conjugated form, UA glucuronide (Extended Data Fig. 1a,b), confirming its bioavailability.

Primary outcome: CD3⁺ immune subpopulations

The primary aim of the present study was to assess the effect of UA on CD3⁺ T cell subpopulations. In addition to growing evidence from recent omics-based studies supporting the notion of aging-associated remodeling of immune populations[31,32], initial observations have highlighted the correlation of a reduced lymphocyte count in the peripheral blood with age[33]. We therefore performed clinical hemocytometry to first categorize circulating immune cells, comparing immune composition at baseline and upon the last study visit (Extended Data Fig. 1c). After 28 days participants in the UA group displayed significantly more circulating lymphocytes (Extended Data Fig. 1d) compared to baseline levels, a change which was not observed in the placebo group. Other immune populations, such as eosinophils, neutrophils, monocytes, and total leukocytes did not show marked alterations upon any intervention (Extended Data Fig. 1e–h).

We then performed broad spectral cytometry (Fig. 2a) to identify cell surface markers and transcription factors (Supplementary Fig. 1). The number of total CD3⁺ αβ, CD8⁺, and CD4⁺ T cells (Fig. 2b–d) among total peripheral blood mononuclear cells (PBMCs) did not change upon taking UA. Yet, we observed a significant change of naive CD8⁺ T cells (T_N) after 28 days of UA intake. (Fig. 2e). The percentage of T_{SCM} remained unaltered (Fig. 2f) in contrast to our previous in vitro observations[29]. Other CD8⁺ T cell subsets, such as central memory cells (T_{CM}), effector memory cells (T_{EM}), terminally differentiated effector memory T cells re-expressing CD45RA (T_{EMRA}) or recently characterized "virtual memory" cells, which arise with a memory-like phenotype without prior foreign antigen challenge[34], remained unaffected in both cohorts (Extended Data Fig. 2a–d). Total CD8⁺ T cells in the UA group displayed more antigen Kiel 67 (Ki-67) (Fig. 2g) after the completion of the last study visit, a marker of cellular proliferation and T cell reinvigoration that predicts pathological complete response to immune checkpoint blockade (ICB) in patients with triple-negative breast cancer[35]. Programmed cell death protein 1 (PD-1) expression was unaltered in both groups (Extended Data Fig. 2e). We also observed a reduction in thymocyte selection associated high mobility group box (TOX) expression (Fig. 2h), the master regulator of T cell exhaustion that marks aging-associated T cells[36] and promotes CD8⁺ T cell dysfunction in cancer[37,38]. There was no difference in prominent senescence markers such as p16 and p21, or KLRG1 and CD57 (Extended Data Fig. 2f–i). Thus, UA altered the CD8⁺ T cell phenotype suggestive of a more naive-like, less exhausted global state. By stark contrast, UA did not affect the phenotype of CD4⁺ T cells in terms of T_N, T_{EM}, T_{CM}, T_{SCM} or T_{EMRA} populations (Extended Data Fig. 2h–l) in our human cohort. There were also no changes in CD4⁺ T helper 1 (Th1) cells (marked by T-bet expression), Gata3⁺ T helper 2 (Th2) cells, FoxP3⁺ T regulatory (T_{reg}) cells, circulating T follicular helper cells (Tfh1, identified via Bcl-6), or γδ T cells (Extended Data Fig. 2m–p). Collectively, UA supplementation instigates phenotypical changes in circulating T cells, with expansion of lymphocyte populations and an emphasis on naive-like, less exhausted CD8⁺ state.

Primary outcome: metabolic reprogramming

The immune system exhibits a striking metabolic plasticity while metabolic reprogramming critically instructs but also defines immune fate and function[14]. For instance, different metabolic needs are met by diverging mitochondrial ultrastructures in T cells[17], which we expected to undergo change upon UA supplementation. A co-primary outcome therefore constituted changes in metabolic dependencies of immune (primarily T cell) populations. To further characterize the metabolic profile of immune cells on a single-cell resolution, we used single-cell

https://doi.org/10.1038/s43587-025-00996-x

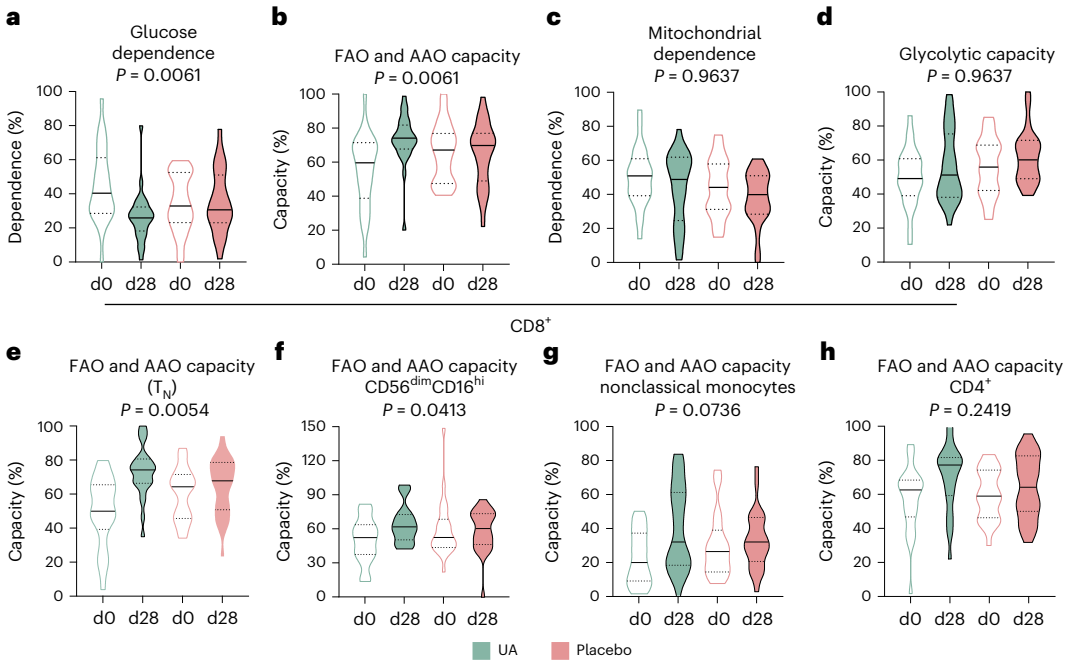

Fig. 3 | Primary end point—UA induces metabolic reprogramming of human immune cells. a–**d**, Metabolic profiling of CD8$^+$ cells using SCENITH. Truncated violin plots of glucose dependence (**a**), fatty acid and amino acid oxidation capacity (FAO and AAO capacity) (**b**), mitochondrial dependence (**c**), and glycolytic capacity (**d**) are shown. Data shown from UA- and placebo-treated participants at baseline (d0) and after the 28 day supplementation period (d28) depicting percentage. Mean (solid line) and 25th/75th quartiles (dotted lines) are shown. $N = 25$ per group. P values for treatment effects were calculated using a repeated measures mixed-effects model. **e**–**h**, Truncated violin plots depicting fatty acid and amino acid oxidation (FAO and AAO) capacity from several immune subpopulations as assessed by SCENITH. Data from T_N (**e**), CD56^{dim}CD16^{hi} NK cells (**f**), nonclassical monocytes (**g**), and CD4$^+$ cells (**h**) are shown from UA- and placebo-treated participants at baseline (d0) and after the 28 day supplementation period (d28). Depicted are mean (solid line) and 25th/75th quartiles (dotted lines), $n = 25$ per group. P values for treatment effects were calculated using a repeated measures mixed-effects model. All statistical tests were two-sided. No adjustments for multiple comparisons were made.

energetic metabolism by profiling translation inhibition (SCENITH), a flow-cytometry-based strategy that uses incorporation of puromycin to infer metabolic dependencies[39]. We first modeled mitochondrial dependence, glucose dependence, glycolytic capacity, and fatty acid oxidation (FAO) and amino acid oxidation (AAO) capacity in CD8$^+$ T cell subsets of all participants at baseline. In line with previous results using SCENITH, the expression of CD45RA, mostly present in naive T cells, is indicative of strong dependence on oxidative phosphorylation (OXPHOS) (Extended Data Fig. 3a,b)[40,41]. After strong metabolic activation of T cells upon antigen encounter[14], memory T cells rewire their metabolism toward a more quiescent but metabolically primed state, shifting toward catabolic processes of generating energy. Correspondingly, we found both elevated glycolytic capacity and FAO and AAO capacity in T_{CM} (Extended Data Fig. 3c,d). Indeed, T_{CM} were significantly less dependent on glucose (Extended Data Fig. 3a), consistent with their induction and maintenance of mitochondrial biogenesis that reflects their ability to create energy via OXPHOS[42]. Thus, our approach faithfully detects metabolic dependencies of immune cell subsets, enabling us to study intervention-related effects.

We next assessed whether UA supplementation provokes changes in immune metabolism. After the 28 day intervention period, CD8$^+$ T cells of the UA group displayed reduced glucose dependence and increased FAO and AAO capacity, whereas it did not elicit changes in mitochondrial dependence or glycolytic capacity (Fig. 3a–d). The capacity to use FAO and AAO was most strongly elevated in naive CD8$^+$ T cells (Fig. 3e and Extended Data Fig. 3e–g). Also, natural killer (NK) cells displayed enhanced FAO and AAO capacity and concomitantly reduced glucose dependence (Extended Data Fig. 3h), while we observed a similar trend in nonclassical monocytes (Fig. 3f and Extended Data Fig. 3i). No statistically significant changes were observed in CD4$^+$ T cells (Fig. 3h and Extended Data Fig. 3k) or B cells (Extended Data Fig. 3h–l). The strong glycolytic phenotype of classical monocytes remained unaltered (Extended Data Fig. 3m,n). Altogether, daily intake of UA resulted in reduced glucose dependence and pronounced capacity to meet bioenergetic needs via the mitochondrial oxidation of fatty acids and amino acids in the lymphoid compartment, consistent with their phenotypical remodeling.

Secondary outcomes: effect of UA on other immune populations and mitochondrial remodeling

A secondary outcome constituted shifts in circulating immune cells frequencies apart from the T cell population.

In addition to the pronounced changes observed in the CD8$^+$ compartment, other peripheral immune populations were also affected by UA supplementation. CD56^{dim}CD16^{bright} NK cells, the most common NK subset in human blood, were expanded among total PBMCs in the UA group (Fig. 4a), while we did not observe a change in the expression of their inhibitory receptors such as NKG2A, KIR, or KLRG1 (Extended Data Fig. 4a–c). Furthermore, we found that the percentage of nonclassical monocytes (defined as CD14^{lo}CD16^{hi} cells) in PBMCs was increased after 28 days of UA compared to placebo (Fig. 4b), whereas the relative frequency of intermediate monocytes and classical monocytes did not differ between the two groups (Extended Data Fig. 4d,e). Yet, classical monocytes exhibited less human leukocyte antigen-DR isotype (HLA-DR) in participants of the UA group at the final study visit (Fig. 4c), indicative of a less inflammatory phenotype[43]. Circulating dendritic cells (DCs) and innate lymphoid cells did not change upon either intervention (Fig. 4d and Extended Data Fig. 4f), and also, the percentage of total B cells, plasma cells, plasmablasts, or specific

https://doi.org/10.1038/s43587-025-00996-x

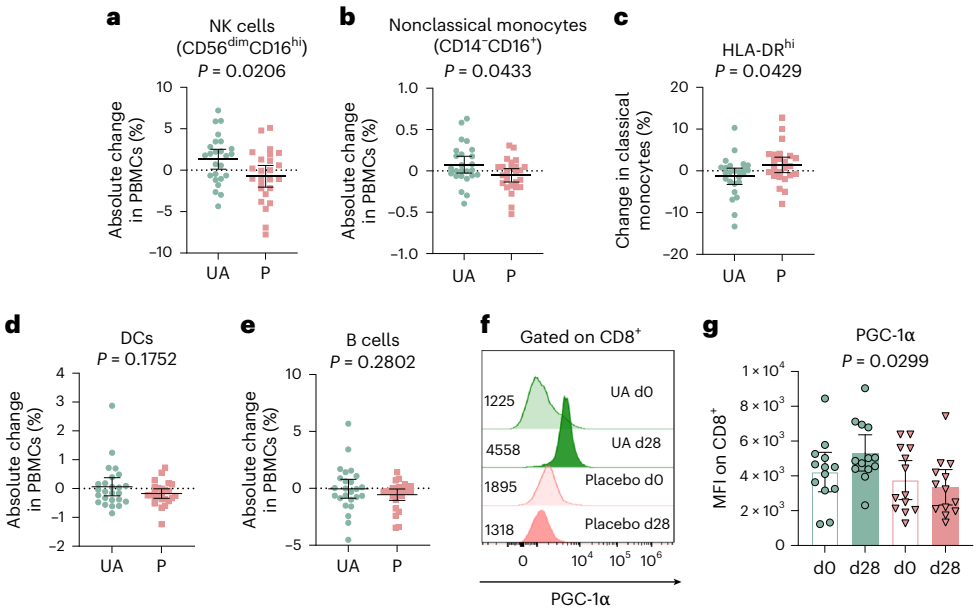

Fig. 4 | Secondary end point—UA alters peripheral immune frequencies and mitochondrial remodeling. a, Absolute change in percentage of CD56^{dim}CD16^{hi} NK cells in PBMCs after 28 days. Data are mean ± 95% CI, $n = 25$ per group. *P* value for treatment effects was calculated using a two-sided repeated measures mixed-effects model. **b**, Absolute change in percentage of nonclassical monocytes (CD14$^-$CD16$^+$) within PBMCs after 28 days. Data are mean ± 95% CI, $n = 25$ per group. *P* value for treatment effect was calculated using a two-sided repeated measures mixed-effects model. **c**, Absolute change in HLA-DR^{hi} cells within classical monocytes after 28 days of UA or placebo supplementation. Data are mean ± 95% CI, $n = 25$ per group. *P* value for treatment effect was calculated using a two-sided repeated measures mixed-effects model. **d**,**e**, Absolute change in percentage of DCs (**d**) and B cells (**e**) within PBMCs after 28 days. Data are mean ± 95% CI, $n = 25$ per group. *P* values for treatment effect were calculated using a two-sided repeated measures mixed-effects model. **f**,**g**, Expression of PGC-1α in CD8$^+$ cells before (d0) and after (d28) UA and placebo supplementation, respectively. Assessed by flow cytometry, data shown as mean fluorescence intensity (MFI). Representative histograms are shown in (**f**), data depicted in (**g**). Data are mean ± 95% CI, $n = 12$ per group. *P* value for treatment effect was calculated using a two-sided repeated measures mixed-effects model. No adjustments for multiple comparisons were made.

B cell subsets was not different between the two intervention groups (Fig. 4e and Extended Data Fig. 4g–j). Collectively, UA supplementation instigates phenotypical changes extending beyond CD8$^+$ immunity.

Considering the well-established yet rapid impact of UA on mitophagy[25] and the association between mitochondrial plasticity and immune fate[17,29,44], which we have previously extended to the notion of UA-elicited mitophagy altering T cell function in mice[29], we next assessed whether UA supplementation elicits mitochondrial remodeling in the immune compartment of humans. To this end, we used MitoTrackerGreen, a fluorescent dye that stains mitochondria independent of mitochondrial membrane potential (MMP). Neither CD8$^+$ or CD4$^+$ cells of UA-treated participants exhibited a change in mitochondrial mass after 28 days (Extended Data Fig. 5a–d). Mitochondrial biogenesis and mitophagy are closely interlinked[15] to guarantee sustained replacement of dysfunctional mitochondria and maintain adequate mitochondrial mass. PGC-1α is considered the master regulator of mitochondrial biogenesis[45]. We have previously shown that UA elicits mitophagy quickly in T cells ex vivo, which is followed by PGC-1α-mediated mitochondrial biogenesis[29]. We therefore hypothesized that an unchanged mitochondrial mass in T cells of UA-treated participants may be due to compensatory mitochondrial biogenesis upon mitophagy induction. Indeed, UA-exposed CD8$^+$ T cells displayed stronger expression of PGC-1α after the intervention period (Fig. 4f,g), whereas no such change was detected after intake of placebo. Consistent with no alterations in the CD4$^+$ phenotype, no significant induction of PGC-1α was seen in CD4$^+$ T cells (Extended Data Fig. 5e). Given that hyperpolarized mitochondria can be a source of reactive oxygen species which can potentiate senescence[46], we finally assessed MMP, where we found no difference in MMP in both CD8$^+$ T cells and CD4$^+$ T cells in the UA group compared to placebo (Extended Data Fig. 5f–h). As we hypothesized that mitophagy induction might have occurred before our follow-up visits, we performed additional ex vivo experiments from PBMCs derived from healthy donors that were not included in the trial. Here, incubation with UA at 25 µM led to quick hypopolarization of mitochondria, followed by lysosome formation, reduction of MitoTracker staining, and mtDNA/nuDNA (mitochondrial DNA to nuclear DNA) ratio, as well as stabilization of Pink1/Parkin levels (Extended Data Fig. 6a–f). This is consistent with rapid mitophagy induction that we have also observed in mice[29]. In summary, our data indicate that the mitophagy inducer UA supplementation affects mitochondria in CD8$^+$ cells in vivo, possibly via PGC-1α-mediated mitochondrial biogenesis.

Secondary outcome: systemic inflammation and activation-induced immune response

Considering the effects of UA on immune polarization and the observation that aging-associated metabolic failure profoundly contributes to the phenotype of inflammaging[18], we next investigated whether circulating cytokine plasma levels are affected by UA supplementation. Sample limitation allowed the measurement of up to $n = 20$ cytokine levels per group. Here, while administration of UA led to significantly lower levels of IL-2, there was no pathological induction of several pro-inflammatory cytokines (Fig. 5a).

A recent single-cell atlas of healthy human blood has indicated an aging-associated bias toward type 2 immunity that is uncovered in healthy participants upon antigen challenge, but not at steady state[32]. We therefore next focused on cytokine expression of stimulated T cells to detect potential differences in the context of immune response which could constitute a potential predisposition to conditions that may only manifest when specifically triggered (such as a pathological type 2 reaction observed in fibrotic conditions). To this end, PBMCs from both intervention groups were incubated in the presence of anti-CD3/anti-CD28 stimulation beads for a total of 4 days (Fig. 4b). Intriguingly, challenged CD8$^+$ T cells of UA-treated

https://doi.org/10.1038/s43587-025-00996-x

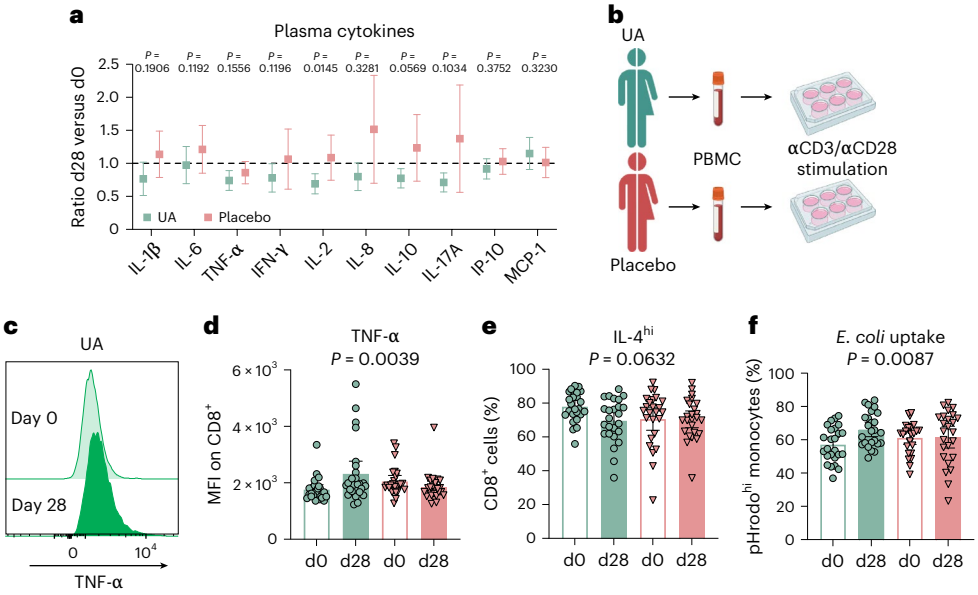

Fig. 5 | Secondary end point—UA alters inflammatory immune response. **a**, Plasma cytokine measurements. Fold change compared to baseline plasma levels of the indicated cytokines of UA- and placebo-treated participants are shown. Data are mean ± 95% CI, n = 15/19/20/20/19/19/19/18/20/20 of matched samples per cytokine. P values for treatment effects were calculated by a two-sided repeated measures mixed-effects model. No adjustments for multiple comparisons were made. **b**, PBMC stimulation overview. Thawed PBMCs from UA- and placebo-treated individuals were stimulated with anti-CD3/anti-CD28 beads for a duration of 4 days, followed by functional readouts. **c**,**d**, Expression of TNF in CD8$^+$ cells before (d0) and after (d28) UA and placebo supplementation, respectively. Cells were stimulated as depicted in **b**. Assessed by flow cytometry, data shown as MFI. Representative histograms are shown in **c**, data is depicted in **d**. Data are mean ± 95% CI, n = 25 per group. P value for treatment effects was calculated by a two-sided repeated measures mixed-effects model. **e**, Percentage of IL-4^{hi} cells within CD8$^+$ cells after 4 days of PBMC stimulation as depicted in **a**. Data are mean ± 95% CI, n = 25 per group. P value for treatment effects was calculated by a two-sided repeated measures mixed-effects model. **f**, *E. coli* uptake of monocytes from UA- and placebo-treated participants before (d0) and after the supplementation period (d28), respectively. Data are mean ± 95% CI, n = 25 per group. P value for treatment effects was calculated by a two-sided repeated measures mixed-effects model. No adjustments for multiple comparisons were made. Schematic in **b** created using BioRender.com.

participants more readily produced TNF while not pathologically enhancing IL-4 secretion, whereas placebo intake did not elicit any changes (Fig. 4c–e). Taken together, our results indicate that UA treatment improves an activation-induced type 1 response, while not influencing inflammatory conditioning at steady state.

Expanding on our functional findings in CD8$^+$ T cells, we next assessed myeloid function after UA. The immunosenescent phenotype is considered responsible for an increased susceptibility to infections in older adults[6]. Given the established role of UA in instructing macrophage polarization in vitro[47] in addition to here suggesting altered circulating monocyte composition, we lastly performed a phagocytosis assay to assess whether UA impacts monocyte phagocytic capabilities of Gram-negative bacteria. Monocytes from UA-exposed participants markedly enhanced phagocytosis of *Escherichia coli* particles ex vivo when compared with the placebo cohort (Fig. 5f), hinting at superior uptake and clearance of Gram-negative bacteria. Collectively, our data support the notion that apart from profound phenotypic and metabolic changes in the human immune system, UA supplementation results in changes in immune function that potentially carries systemic consequences.

Exploratory outcome: single-cell RNA sequencing

To further profile the immune compartment upon UA intake, we performed explorative single-cell RNA sequencing (scRNA-seq) from five participants before and after both interventions. After quality control filtering, we profiled a total of 231,079 cells with >1,000 genes per cell (Extended Data Fig. 7a). For population clustering, a hierarchical approach was used[32] incorporating Azimuth[48] to define subpopulations (Extended Data Fig. 7b). A total of 89 genes were differentially expressed in CD8$^+$ T cells (52 up, 37 down) after 28 days of UA compared to placebo (Extended Data Fig. 7c). Consistent with previous in vitro data[29] and our findings of UA eliciting a naive-like state in T cells (Fig. 2), we found upregulation of the Wnt-associated stemness transcription factors *TCF7* and *LEF1*, as well as induction of *IL7R*. Among downregulated genes, several genes associated with T cell exhaustion, suppression, and hypofunction (*NR4A2*, *CREM*, *TGFB1*, *METRNL*)[49–52] were identified. Canonical pathway analysis revealed activation of T cell receptor (TCR) signaling and several pathways associated with cytoskeleton remodeling, adhesion, and cellular motility (Extended Data Fig. 7d) in UA-exposed CD8$^+$ T cells. Likewise, Gene Ontology enrichment analysis using EnrichR[53] confirmed similar tendency toward cytoskeletal reorganization programs (Extended Data Fig. 7e). Among downregulated canonical pathways, both protein kinase A (PKA) signaling and other immune inhibitory pathways were shown to be strongly inhibited (Extended Data Fig. 7f). Indeed, recent findings suggest G-protein coupled receptors (GPCRs) and Gα_s signaling as an immune checkpoint in human cancer that drives a hyporesponsive state, thereby resulting in immunotherapy failure[54]. Consistently, predicted upstream regulators suggested a reduced role of several components of the GPCR–Gαs–PKA axis, such as G protein-coupled receptor 174 (GPR174), guanine nucleotide binding protein (G protein), alpha stimulating (GNAS), and cyclic adenosine monophosphate (cAMP; Extended Data Fig. 7g). Other transcription factors central to T cell exhaustion and blunted tumor infiltration such as interferon regulatory factor (IRF4; ref. 55), signal transducer and activator of transcription 6 (STAT6) and yes-associated protein 1 (YAP1) were also among predicted inhibited pathways. These findings extended to the T_{EM} subset where we also observed downregulation of the transcription factor 'cAMP-responsive element modulator' (CREM; Extended Data Fig. 7h,i). Gene Ontology enrichment analysis confirmed an upregulation of cytoskeletal and adhesion-associated programs, while revealing downregulation of GPCR–Gαs–PKA-associated

pathways and its ligand PGE_2 in T_{EM} as well. Among naive T cells, several components of the electron transport chain (*MT-ND5*, *MT-CO1*, *MT-CO2*) were induced upon UA intake (Extended Data Fig. 7j). Collectively, the transcriptomic findings support our experimental evidence of altered mitochondrial activity and reduced $CD8^+$ T cell suppression upon UA intake.

Changes in the NK cell compartment in UA-treated individuals were characterized by reduction of several well-known immediate-early genes[56] (Extended Data Fig. 8a) including *NR4A2*, *DUSP1*, *FOS*, *JUN*, and *NFKBIA*. These constitute primary response genes that are induced rapidly after stimulation and generally do not require de novo protein synthesis[57]. Consistently, other downregulated genes belonged to inflammatory TNF and interferon pathways, while NK cells of UA-treated participants also displayed reduction of the activation markers *CD69* and *CXCR4* (Extended Data Fig. 8a). Such transcriptional profile is in line with less "inflamed" NK subsets that were recently described[56]. Furthermore, NK cells also displayed an upregulation of cytoskeletal and adhesion genes. In line with a more mature NK state, upregulated genes included *NEAT1* and *CD160*, thereby reflecting a recently proposed NK1(B) profile[58]. Consistently, Gene Ontology enrichment analysis revealed distinct functional and spatial specializations associated with NK1 cells such as cytoskeletal remodeling, adhesion, and membrane–protein interactions. By contrast, NK cells of UA-receiving participants were less linked to an inflammatory response and nitrogen-associated pathways (Extended Data Fig. 8b,c).

Monocytes displayed a strong upregulation of several mitochondrial genes (*MT-CYB*, *MT-ND5*, *MT-ATP8*, *MT-CO1* among others; Extended Data Fig. 8d) as well as nicotinamide phosphoribosyltransferase (NAMPT), the rate-limiting enzyme of the nicotinamide adenine dinucleotide (NAD) salvage pathway that is required to establish an anti-inflammatory M2-like (alternatively activated) polarization[59]. Strongest downregulation was observed among genes that belonged to the interferon response pathway (for example, *IFITM2*, *IER2*, *STAT1*; Extended Data Fig. 8d,e). Interferon-associated and inflammatory pathways were thus predicted as negative upstream regulators, whereas inhibitors of pathogenic myeloid-derived inflammation such as ETS variant transcription factor 3 (ETV3), ETV6 and Cbp/P300-interacting transactivator with Glu/Asp-rich carboxy-terminal domain 2 (CITED2; refs. 60,61) were assumed to be activated upstream regulators (Extended Data Fig. 8f). The transcriptomic characterization therefore reinforces the notion of an anti-inflammatory monocyte polarization under UA treatment. In line with this, downregulated genes by UA in B cells included an inflammatory gene signature (*MX1*, *XAF1*, *ISG15*, *TNSF10*; Extended Data Fig. 8g) observed in patients with SARS-CoV2 (ref. 62). Accordingly, downregulated pathways included hypercytokinemia during viral infections, while B cells displayed upregulation of B cell receptor (BCR)-associated pathways (Extended Data Fig. 8h,i). $CD4^+$ T cells were largely characterized by a signature associated with mitochondrial health (Extended Data Fig. 8j–l), suggesting that $CD4^+$ cells are also affected by UA, in line with trends on PGC-1α expression and metabolic remodeling. Taken together, our explorative scRNA-seq data indicated that UA induces a substantial change in immune cell transcriptional profiles, with impact on pathways related to inflammation and cellular and mitochondrial metabolism. This is in line with the reduction of immune aging phenotypes described above, further underscoring the UA-dependent potentially beneficial transcriptomic alterations in the human immune system.

Discussion

The past century has seen a progressive demographic shift with an increase of life expectancy, resulting in an expected doubling of the population aged over 60 years by 2050 (ref. 63). Yet, interventions to reliably extend healthspan, that is, years of life without chronic conditions, are still lacking. Maintaining immune health plays a crucial role in extending healthspan, as a well-functioning immune system is essential for preventing infections, reducing inflammation, and controlling the onset of age-related diseases. Indeed, higher levels of systemic inflammation and immune dysfunction observed in older adults favor T cell dysregulation, with cytokine storms in infectious disease, as recently observed in the COVID-19 pandemic[64,65], or blunted immune response to cancer[66]. We here provide evidence that supplementation with UA alters immune phenotype and function, highlighting the potential capacity of mitophagy-inducing agents to effectively and safely alter the human immune system.

Adaptive immune cells have emerged as central drivers of aging-associated inflammation[67], with metabolic changes in immune cells promoting multimorbidity[18]. The present study was designed to prospectively investigate changes in the T cell populations and their metabolic functions upon UA supplementation in an immune-aged population (>45 years). Indeed, we found an expansion of circulating naive $CD8^+$ T cells in the UA study group, consistent with our previous in vitro findings[29]. It is worth noting that the reduction of this population represents one of the main alterations during immune aging[31,36,47]. $CD8^+$ T_{SCM} remained unaltered, in contrast to UA's ability to potently induce this long-lived subset ex vivo to potentiate cellular therapies[29]. However, it is important to note that the circulating T_{SCM} population is thought to be strikingly stable throughout age[68]. Whereas a growing number of approaches has been identified to expand human T_{SCM} in vitro[69], no validated strategies to expand T_{SCM} in humans have been identified yet.

Mitochondrial dysfunction and reduced autophagic capacities are well-established hallmarks of aging[16]. Therapeutic targeting of these limitations by inducing mitophagy via direct UA supplementation[25,26] has been shown to be an attractive strategy to improve muscle function in older adults[27,28]. In the immune system, alterations in mitochondrial structure and dynamics critically shape immune cell fate and function[17,29,44]. Indeed, we have observed mitochondrial and metabolic remodeling in T cells after UA intake, characterized by increased PGC-1α expression indicative of mitochondrial biogenesis and enhanced capacity to oxidize fatty acids and amino acids to meet bioenergetic needs. It is important to note that we did not formally investigate the activation of classical mitophagy or autophagy programs in this trial, such as an increase of the Pink1/Parkin machinery. Yet, we have previously delineated the mechanism of UA on murine T cells, highlighting the initiation of Pink1-mediated mitophagy within the first 6 h of UA exposure that results in subsequent Wnt/β-catenin signaling, TCF1 expression, and feedback mitochondrial biogenesis[29]. We also confirm these findings in human immune cells here, as we observe that mitophagy can be observed ex vivo within 48 h. Yet, our in vitro experiments use much higher concentrations than the physiological levels achieved in the clinical setting. However, as we observe elevated PGC-1α protein levels, metabolic features resembling a rejuvenated mitochondrial phenotype and an increase of TCF7 (encoding TCF1) expression in our sequencing data, we propose that a similar mechanism to our previously defined sequence may govern UA-mediated T cells in vivo. Apart from the discussed role of UA shaping T cell response, preclinical evidence has shown a role of UA in instructing macrophage polarization in vitro, in turn fostering an anti-inflammatory phenotype[70]. Concomitantly, we here show that systemic UA application renders a less inflammatory monocyte phenotype in humans while improving experimental phagocytosis of *E. coli*, which is consistent with the requirement of adequate mitochondrial dynamics for macrophages to respond to a bacterial challenge[71]. Further mechanistical studies are, however, required to fully understand how mitophagy shapes host response to bacterial challenge or how it affects other immune cells under experimental conditions. This will prove key to assess whether instructing mitochondrial remodeling represents a generally attractive therapeutic option for humans that extends beyond the effect of UA.

In addition to deeply characterizing the effects of UA on the human immune system in a placebo-controlled manner, thereby providing evidence for potentially ameliorating inflammaging, our work proposes future hypothetical applications that now warrant further investigation. While previous experimental studies have highlighted the role of mitochondrial dynamics and T cell longevity in sustaining an antitumor response[19,20,29], several lines of clinical evidence suggest that an aged immune system and mitochondrial dysfunction impair cancer survival in humans, which may be targeted by UA supplementation. For instance, circulating T cell immunosenescence is observed in patients with non-small cellular lung cancer, correlating with resistance to ICB, but not conventional chemotherapeutic regimens[72]. Likewise, retained Ki-67$^+$ expression in CD8$^+$ cells has been associated with ICB response in triple-negative breast cancer[35]. Moreover, mitochondrial repression is observed in tumor-infiltrating lymphocytes of patients with head and neck squamous-cell carcinoma, correlating with the upregulation of coinhibitory markers[20]. Mechanistically, PD-1 engagement suppresses PGC-1α expression in CD8$^+$ T cells that drives mitochondrial insufficiency[73]. Whereas mitochondrial metabolism is critical for CD8$^+$ T cell migration within tumors[74], we show improved OXPHOS capacity and induction of a transcriptional program pertaining to homing and adhesion upon UA intake. Given that our phenotypical, metabolic, functional, and transcriptional findings address several critical characteristics pertaining to T cell dysfunction, hypo-responsiveness, and ICB resistance in cancer, future studies should focus on how UA shapes the immune system in patients with systemic malignancy and how it can be potentially harnessed to enhance response to immune-based therapies.

Despite meeting its designed primary outcomes and several secondary end points, thereby proposing UA as an attractive option to alter immune aging, we acknowledge certain limitations of the present study. Whereas our findings provide clear evidence of reduced immune aging features, further studies are required to examine whether these improvements induced by UA translate into clinically tangible benefits, such as reduced occurrence of infectious diseases, a boost in vaccination responses in older adults or augmented responses to cancer therapies. This is especially of importance as both age-related distributional dynamics and functional relevance of several immune populations, such as CD14^{lo}CD16^{hi} monocytes and CD56^{dim} NK cells studied here, remain unclear[9,32]. Given that sample limitations only enabled the assessment of cytokine levels for a maximum of $n = 20$ participants, this part of the study remains underpowered. We observed trends for several pro-inflammatory cytokines at steady state, which ultimately failed to achieve statistical significance using the mixed effects model applied here. However, these trends are in line with a previous trial in 25 UA-treated adults, where a significant reduction of IFNγ, TNF, and IL-1β was observed[27]. In addition, scRNA samples were selected based on their post-randomization response, meaning that the comparisons here do not respect randomization and are to be considered of explorative nature. Likewise, corrections for multiplicity were made, and secondary analyses should be interpreted with caution. We do not report the pre-specified secondary end point of epigenetic age of PBMCs, as these data were analysed after unblinding. As this was a pilot study seeking to confirm the effects observed in murine models[29], we did not perform a dose escalation. However, other studies have established an optimal intake dose for sufficient UA metabolite levels[75] which is in line with the dose used for this trial. Our study confirmed that robust immune remodeling is quickly induced after a 28 day intervention period, although we did not perform a long-term follow-up after successful intake, for example, after several months. Consequently, it is worth further investigating the longer-term health impact of UA supplementation on immune aging including also older individuals. Such questions are of great importance when assessing the clinical value of UA, as we propose further investigating a potential role as a partner for cancer immunotherapy. In the same line, it is worth exploring in future trials the exact timepoint that UA-mediated immune remodeling starts to occur.

Collectively, our data provide strong evidence that altering mitochondrial dynamics via the orally available and well-tolerated mitophagy inducer UA elicits systemic immune remodeling and potentially reduces the immune aging phenotype. We therefore provide an intervention-based approach to limiting immune aging that may have potential to benefit chronic conditions characterized by immune dysfunction.

Methods

Experimental model and participant details

Trial design and study schedule. The present study (MitoImmune) is a randomized, double-blind, placebo-controlled interventional study including healthy participants. Participants were randomized to receive either UA (Mitopure, Amazentis SA) orally at a daily single dose of 1,000 mg ($n = 25$) or a corresponding placebo ($n = 25$; containing lecithin, medium-chain triglycerides, and glycerol monostearate without Mitopure) for a duration of 28 days. The daily dose of 1,000 mg UA is consistent with doses used in previous clinical trials assessing muscle function. Consolidated standards of reporting trials (CONSORT) diagram for participant inclusion is depicted in Fig. 1. The study was approved by the local institutional review board (IRB) of the University of Frankfurt, Germany (Ethikkommission des Fachbereichs Medizin der Goethe-Universität, approval number 2022-745_2). Participants were recruited at the clinical site (Goethe University Hospital Frankfurt, Department of Medicine I) via paper-based flyers and social media campaigns. Recruitment was initiated in March 2023, and the last participant completed the last visit in December 2023. A total of 79 potential participants were screened for eligibility, of which $n = 50$ met all the inclusion and exclusion criteria and were subsequently randomized. Participants underwent three study visits at baseline, after 7 days (d7) and after 1 month (d28), respectively. Blood was drawn on all study visits as depicted above, and adverse events were recorded. Participant demographics are displayed in Table 1. All participants ($n = 50$) completed the outlined study visits, but one participant of the placebo group ($n = 1$) discontinued the allocated intervention prematurely. No new concomitant diets or medications were reported. All 50 participants are included in the final analysis for the primary end point of the trial as established by the study protocol. Primary end points constituted changes in percentages of CD3$^+$ T cell immune cell populations (in particular, CD8$^+$ naive T cells and CD8$^+$ T_{SCM}) and changes in mitochondrial activity in CD3$^+$ T cells as assessed by flow cytometry. We have deviated from the initial intention of using real-time metabolic profiling of immune cells (such as Seahorse), as SCENITH allows a more granular subset-specific analysis of immune metabolism using low number of cells. No other deviations from the study protocol were made, and no new IRB approval or power calculations were required for this change. Secondary end points were the following: change in pro- and anti-inflammatory cytokine levels (IL-6, TNF, IL1-β, IL-10) in plasma, change in percentages of other immune cell populations (B cells, NK cells, macrophages, DCs, and so on) via flow cytometry, change in mitochondrial content of CD3$^+$ T cell populations via MitoTracker staining using flow cytometry, changes in gene expression measured via single-cell analysis of CD3$^+$ T cells, change in PBMC immune function, changes in lipid profile, and number of adverse events. We will report the pre-specified secondary end point of epigenetic age of PBMCs separately, as these data were analysed after unblinding of the group allocation. Analysis was conducted by the original group assignment, and every study participant was enrolled using the same study protocol version. The study was registered before start of recruitment (https://clinicaltrials.gov/study/NCT05735886; registration date 21 February 2023) and was conducted in accordance with the guidelines of the International Council of Harmonization for Good Clinical Practice and

the Declaration of Helsinki. The present trial follows the CONSORT reporting guidelines for randomized clinical trials.

Inclusion and Exclusion criteria. All study participants provided written informed consent before undergoing randomization. Participants were generally healthy as assessed by a study physician to exclude participants with underlying chronic conditions that may influence the immune system. Study participants were aged between 45 and 70 years and of average body weight (BMI between 20.0 and 34.99 kg m^{-2}). Participants received a travel compensation established by the IRB.

Participants agreed to avoid excessive physical activity for the duration of the trial or change their regular diet. Likewise, participants agreed to refrain from starting other dietary supplements for the duration of the trial. Concomitant use of corticosteroids, antibiotics, any anabolic steroid, creatine, protein supplements, casein or branched-chain amino acids, immune-boosting (vitamin C, zinc) or mitochondrial (COQ10, NAD+) supplements within 45 days before screening disqualified trial participation. Smoking and excessive alcohol use, as defined by current WHO criteria, constituted exclusion criteria. In addition, other exclusion criteria included chronic conditions that may have metabolic consequences, are thought to promote inflammation, or have an effect on trial product absorption (such as gastrointestinal conditions) as assessed by a study physician. The study only included participants that met all inclusion and exclusion criteria (healthy, aged adults), and the results may not generalize to other diseases or age groups.

Method details

Product intake and randomization. The investigational product was labeled according to International Council of Harmonization for Good Clinical Practice guidelines and local regulatory specifications and requirements.

The investigational product was provided as a maximum of four softgels, with each softgel containing 250 mg UA or placebo. UA or placebo softgels were packaged into bottles by Patheon Softgels B.V., each bottle containing 30 softgels. For the purpose of the study, the participants were therefore expected to take four softgels on each day. Each participant received four bottles for a 28 day supply at the start of the study.

The investigational product was blinded into a study code by an unblinded person at the sponsor site, who was not involved in trial design, data collection, analysis, or interpretation of the data. Upon study participant inclusion and informed consent, randomization was performed double-blind at the study site, using the eCRFs (electronic case report forms) (Secutrial) web-based, in-built randomization platform. A static stratified block randomization algorithm was used, randomizing participants according to age, sex, and BMI. For this block-based randomization strategy, a block size of four was used. All participants received the allocated intervention. Participants and providers were therefore blinded to the intervention.

Compliance. Compliance was assessed by counting the returned unused test product at the final visit. Compliance was calculated within the eCRF, dividing the number of dosage units taken by the number of dosage units expected, followed by multiplication by 100. Whenever unused test product was unavailable due to participants' inadvertent discarding of the softgel-containing capsules, participants were asked to specify their compliance.

Adverse event reporting. Participants were instructed to contact the principal investigator (that is, the lead study physician) as soon as possible if he or she has noticed a problem with the investigational product to enable direct assessment of the situation. Otherwise, participants were asked for any new adverse events during the regular study visits. All adverse events were categorized by the Common Terminology Criteria for Adverse Events version 5.0, which are displayed in Extended Data Fig. 2. No life-threatening adverse events were recorded.

Data management. Study data were processed in accordance with the principles of good clinical practice. Data were acquired from source documentation and entered for each individual participant eCRF into a validated data management system (Secutrial). Data entry was completed by site personnel into the study database system. Reference ranges were provided to query each laboratory parameter used during the study to identify the out-of-range values. The study blind was broken at the end of the study following blind database review. Emergency unblinding for safety reasons was not required during the conduct of the study. Source documents were reviewed to ensure that all items had been completed and that the data provided are accurate and obtained as specified in the protocol.

Laboratory chemistry/hematology. During the baseline and follow-up visits, blood was drawn by a physician or physician's assistant to assess blood biochemistry parameters and hematology. Analysis was performed using clinically validated systems at the University Hospital Frankfurt, Germany.

Bioavailability assessment of UA. Plasma concentrations of parent UA and its conjugated form, UA-glucuronide, were analysed before and after the 28 day intake period as previously described[25]. All values below the limit of quantification were set to 0.

PBMC isolation. Peripheral blood (35 ml) was collected by venous puncture into EDTA-buffered collection tubes. EDTA tubes were then spun at 400 *g* for 5 min at room temperature to separate plasma from cellular contents. Plasma was immediately frozen and kept at −80 °C for experiments detailed below. Resulting cells were subsequently diluted in PBMC wash buffer (PBS/2% FCS) and transferred to SepMate tubes (StemCell; 85460) layered with 15 ml FicollPaque Plus (Merck) or LymphoPrep (Progen; 1856-1). PBMC isolation was then performed according to manufacturer's recommendations. Tubes were first spun at 1,200 *g* at room temperature for 10 min. The resulting PBMC layer was then transferred to a new 50 ml tube, filled with 15 ml PBMC wash buffer and spun again at 300 *g* for 8 min. Cell pellets were again washed in PBMC wash buffer and centrifuged at 400 *g* for 5 min. Finally, the resulting pellet was reconstituted in 6 ml of PBMC freezing medium (FCS/10% DMSO), rendering a single-cell suspension with final cell concentration between 1.5×10^6 and 5×10^6 cells per ml. Suspensions were quickly transferred into standard cryogenic vials and cryopreserved in a freezing container at −80 °C overnight. For long-term storage, cells were kept in vapor phase liquid nitrogen.

PBMC thawing. PBMCs were quickly thawed in a 37 °C water bath, then slowly added dropwise into polystyrene tubes containing 1 ml of pre-warmed PBMC medium (DMEM/2% FCS). Empty cryovials were again flushed with warm PBMC medium to collect all remaining cells. Then, tubes were topped to 10 ml of PBMC medium and centrifuged at 500 *g* for 5 min. Cells were counted and used for subsequent experiments.

Flow cytometry staining and data processing. Spectral flow cytometry to broadly analyze immune composition was performed on PBMCs from 25 UA and 25 placebo individuals from our cohort. Flow cytometry staining was performed in three batches to minimize batch-related effects.

PBMC were thawed and allowed to recover for 3 h in uncoated cell culture dishes. All samples for any particular donor series were thawed together. Cells were stained with the panel shown in Supplementary Table 1. For the intracellular panel, cells were stained

after recovery with the surface panel, then fixed and permeabilized using the ThermoFisher Foxp3 Fix/Perm (00-5523-00) system, followed by staining for intracellular markers. For the surface-only panel, cells were treated with Bafilomycin A1 (0.5 µM) for 45 min, followed by 45 min incubation with C12FDG before collection and surface staining. All cells were analyzed on a Cytek Aurora cytometer. FCS files were exported into FlowJo V10.7.2 (BD) for further analysis.

Raw data for all 64 output channels were unmixed using library single-color reference controls for each marker. Spectral compensation for the resulting unmixed data was corrected by manually adjusting a 31 × 31 matrix of spectral overlaps. Once the data were properly compensated, each individual marker was checked for signal and specificity. The resulting data were then manually gated using a representative sample. The gates are then applied to the other samples in the batch while spot-checking the gating of the other samples for consistency with the first sample gated. Exemplary gating strategies are shown in Supplementary Figure 1.

Mitochondrial analysis of PBMCs. PBMCs were thawed as described above and cultured in T cell medium (RPMI (ThermoFisher Scientific) 10% FBS (South America origin), 10 mM Hepes (Sigma), 1× Non-Essential Amino Acid, 1 mM sodium pyruvate, 50 µM β-mercaptoethanol, 100 U ml^{-1} penicillin, 100 µg ml^{-1} streptomycin, and 2 mM Glutamax (ThermoFisher Scientific) overnight. After washing, cells were reconstituted in T cell medium containing the respective staining agent: for labeling of mitochondrial mass, MitoTracker Green (Invitrogen; M46750) was used at a concentration of 40 nM for 30 min at 37 °C. MMP was assessed via MitoTracker Red CMXRos (Invitrogen; M7512; 200 nM, 60 min) due to its retention upon formaldehyde fixation. Cells were then stained with a combination of vFluor 450-conjugated antibody to CD3 (Tonbo Biosciences; OKT3; 1:100), PE-Cy7-conjugated antibody to CD4 (BioLegend; SK3; 1:200), APC-Cy7-conjugated antibody to CD8 (BioLegend; SK1; 1:200), APC-conjugated antibody to CCR7 (BioLegend; G043H7; 1:200), FITC-conjugated antibody to CD45RA (BD; Clone HI100; 100), and Ghost Dye Violet 510 Fixable Viability Dye (Cell Signaling; 59863; 1:1,000). To assess expression of PGC-1α, cells were rested for 4 h after thawing then stained with the panel above for 15 min at 4 °C. After washing in FACS buffer, cells were permeabilized and fixed using the eBioscience Foxp3/Transcription Factor Staining Buffer Set, followed by staining with PGC-1α (Santa Cruz; sc-518025; D-5; 1:50) antibody. For mitochondrial analysis, cells were finally fixed in 1% paraformaldehyde and analyzed on a Cytek Aurora cytometer. Samples were unmixed using reference controls generated in combination with stained Ultracomp beads (Thermo Fisher Scientific, 01-2222-41).

Mitochondrial dependency analysis of immune populations: SCENITH. SCENITH was used to determine metabolic dependencies of select immune populations, SCENITH reagents kit (inhibitors, puromycin, and anti-puromycin clone R4743L-E8) were obtained from www.scenith.com/try-it and used according to the provided protocol. In short, 0.3 × 10^6 PBMCs were treated for 15 min with Control (DMSO), 2-deoxy-glucose (2DG; 100 mM), oligomycin (O; 1 µM) and the combination of 2DG and oligomycin (DGO) or Harringtonine (H; 2 µg ml^{-1}). Following metabolic inhibitors, puromycin (final concentration 10 µg ml^{-1}) was added to cultures for 30 min. After puromycin treatment, cells were washed in PBMC wash buffer and stained with the following antibodies for 15 min at 4 °C: PE-Cy7-conjugated antibody to CD4 (BioLegend; SK3;1:200), APC-Cy7-conjugated antibody to CD8 (BioLegend; SK1;1:200), AF700-conjugated antibody to CD45RA (BD; 150503; 1:100); vFluor 450-conjugated antibody to CD3 (Tonbo Biosciences; OKT3; 1:200), APC-conjugated antibody to CCR7 (BioLegend; G043H7; 1:200), BV786-conjugated antibody to CD14 (MφP-9; 1:200), PE-Cy5.5-conjugated antibody to CD19 (eBioScience; SJ25C1; 1:200), PE-CF594-conjugated antibody to CD16 (BD; 3G8; 1:200), BV711-conjugated antibody to CD56 (BD; NCAM16.2; 1:200), and Ghost Dye Violet 510 Fixable Viability Dye (Cell Signaling; #59863; 1:1,000).

Cells were fixed and permeabilized using the Foxp3 intracellular staining kit for 1 h. Intracellular staining of puromycin and protein targets was performed for 1 h in diluted (10×) permeabilization buffer at 4 °C. Finally, data acquisition was performed using the Cytek Aurora flow cytometer. Samples were unmixed using reference controls generated in combination with stained UltraComp beads using the SpectroFlo (version 3.2.1) software. The unmixed FCS files were used for data processing and analysis using FlowJo (BD, version 10.7.1). Immune cell populations of interest were gated manually for downstream analysis. Geometric mean fluorescence intensity (gMFI) expression values for puromycin were exported from FlowJo to calculate metabolic dependencies. The following calculations were used:

(1) (C = gMFI of anti-Puro-Fluorochrome upon Control treatment)
(2) (2DG = gMFI of anti-Puro-Fluorochrome upon 2DG treatment)
(3) (O = gMFI of anti-Puro-Fluorochrome upon oligomycin treatment)
(4) (DGO = gMFI of anti-Puro-Fluorochrome upon 2DG + oligomycin (DGO) treatment)
(5) (Glucose dependence = 100(C − 2DG)/(C-DGO))
(6) (Mitochondrial dependence = 100(C − O)/(C-DGO))
(7) (Glycolytic capacity = 100 − Mitochondrial dependence)
(8) (Fatty acid and amino acid oxidation capacity = 100 − Glucose dependence)

T cell stimulation assay. To study the antigen response of T cells, 0.5 × 10^6 thawed PBMCs were plated in a 24-well plate for 24 h to deplete monocyte populations by plastic adherence. Next, cells in suspension were transferred to a new tube and centrifuged at 350 *g* for 5 min, followed by reconstitution in fresh T cell medium. Cells were stimulated with human anti-CD3/C28 stimulation beads (Dynabeads, ThermoFisher; 11131D) for 4 days, using a ratio of 25 µl beads per 0.5 × 10^6 cells.

To study cytokine expression, Brefeldin A (Biolegend; 420601) was added to stimulated PBMCs for the last 3 h. Cells were then washed and stained with PE-Cy7-conjugated antibody to CD4 (BioLegend; SK3; 1:200), APC-Cy7-conjugated antibody to CD8 (BioLegend; SK1; 1:200), APC-conjugated antibody to CCR7 (BioLegend; G043H7; 1:200), FITC-conjugated antibody to CD45RA (BD; Clone HI100; 1:200), and Live/Dead Fixable Blue Dead Cell Stain Kit (Thermo Fisher Scientific; L2310; 1:1,000), while intracellular staining for cytokine assessment was performed with BD Cytofix/Cytoperm (BD) with 20 min fixation and overnight incubation with CF594-conjugated antibody to IL-4 (BD; 11B11; 1:300) and APC-conjugated antibody to TNF (BD; MAb1; 1:300). Finally, samples were fixed with 1% paraformaldehyde until data acquisition.

Plasma cytokine measurements. Inflammatory cytokines were measured using LEGENDplex HU Essential Immune Response Panel (BioLegend; 740930) according to the manufacturer's instructions. Technical duplicates were used for both the standard curve and experimental samples. Analysis was performed with the provided software.

Phagocytosis assay. To assess phagocytotic capacity of monocytes, the pHrodo *E. coli* Red BioParticles Phagocytosis Kit for Flow Cytometry (Invitrogen) was used. Thawed PBMCs were immediately used for analysis. *E. coli* Red BioParticles (25 µl) was added to 0.25 × 10^6 PBMCs in 225 µl PBMC medium. As a negative control, 20 µl of PBS was added to 225 µl of PBMCs. Incubation was performed at 37 °C for 45 min, followed by immediate transfer on ice. Cells were then washed in FACS buffer, centrifuged at 500 *g* for 5 min, followed by another wash step. Cells were stained with BUV395-conjugated antibody to CD3 (BD; UCHT1; 1:200), BV786-conjugated antibody to CD14 (BD; MoP9; 1:200), and Live/Dead Fixable Blue Dead Cell Stain Kit

(Thermo Fisher Scientific; L2310; 1:1,000) for 10 min at 4 °C. After washing, cells were reconstituted in PBS and subjected to analysis using a Cytek Aurora flow cytometer. Monocytes were identified as $CD3^{-}CD14^{+}$ cells.

scRNA-seq library preparation. scRNA-seq was performed on PBMCs from 5 UA and 5 placebo individuals from our cohort, using matched samples from baseline visit and after 28 days. The sequencing was performed by Singleron. Cryopreserved human PBMCs were thawed, washed, resuspended in PBS, and counted with the Luna FX7 automated cell counter (Logos Biosystems). The concentration of the cell suspension was adjusted to 4×10^5 cells ml^{-1} with PBS and loaded onto a microfluidic chip (part of Singleron GEXSCOPE Single Cell RNAseq Library Kit, Singleron Biotechnologies) to capture around 10,000 cells. Tagging the cells' transcriptomes was done by loading paramagnetic beads ligated to oligonucleotide barcodes and unique molecular identifiers. The scRNA-seq libraries were constructed according to manufacturer's instructions (Singleron Biotechnologies). The resulting scRNA-seq libraries were sequenced on an Illumina NovaSeq X instrument with a paired-end 150 bp approach by Macrogen Europe. The reads were demultiplexed on Illumina's BaseCloud.

scRNA-seq data filtering, normalization, and batch correction. Count tables were obtained from Singleron (matrix.mtx, genes.tsv, and barcodes.tsv) and imported into R (version 4.2.2) using the Read10X function in Seurat[48,76–78] (version 4.3.0.1). Seurat objects were created using min.cells = 1 and min.features = 500. Metadata such as timepoint, treatment, and donor were added to each Seurat object. Cells with more than 15% mitochondrial content were removed. Each Seurat object was normalized, scaled, and clustered with default settings. Next, DoubletFinder[79] (version 2.0.3) was used with 2.5% expected doublets. Seurat objects were combined into one and were normalized, scaled, and clustered with default settings. Cell cycle scores were generated using the CellCycleScoring function and cc.genes.updated.2019 reference in Seurat to score for S- and G2M-phase. Next, data were normalized with the SCTransform function, method = "glmGamPoi", using all cells and vars.to.regress = c("percent.mt","S.Score","G2M.Score"). To reduce batch effects, Harmony[80] (version 0.1.1) was used with group.by.vars = 'orig.ident'. For final Uniform Manifold Approximation and Projection and clustering, the ElbowPlot function was used to determine the number of principal components and was set to 30.

Cell type calling. For calling cell types, Azimuth[48] (version 0.4.6) with pbmcref.SeuratData (version 1.0.0) and SeuratData (version 0.2.2) was used. Seurat object was subset based on the cell type score from layer 1, predicted.celltype.l1.score > 0.75. Further, the Seurat object was split into several smaller Seurat objects based on cell type identity in layer 1 for $CD8^{+}$ T cells, $CD4^{+}$ T cells, NK cells, monocytes, and B cells. Cells with a score lower than 0.8 were removed, and each Seurat object was normalized with SCTransform, batch corrected with Harmony and clustered as previously described for the whole data set. Cell types were called again on each Seurat object with Azimuth, and only cells that belonged to the correct cell type, this time in layer 2, were kept.

Differential gene expression, gene set enrichment analysis, and Ingenuity Pathway Analysis. Differentially expressed genes (DEGs) for each cell type between timepoint 28 and 0 were obtained with the FindMarkers function in Seurat, with placebo or treated cells, respectively. The Logfc.threshold was set to 0.1 or 0.01, and only genes with p_val_adj below 0.05 were kept.

Further, the clusterProfiler[81] package (part of Bioconductor 3.18) was used in R with gseGO functions to find pathways and Gene Ontology terms for each condition. First, SYMBOL (official gene symbol) was converted to corresponding Entrez gene identifiers (ENTREZID), and genes were ranked based on $\log_2$ fold change. The output with logfc.threshold 0.01 was used, and only pathways and Gene Ontology terms with a P value cutoff = 0.1 were kept.

DEGs with $P < 0.05$ and a $\log_2$(fold change) > 0.1 were selected as input for Ingenuity Pathway Analysis (IPA). IPA was used to identify activated and inhibited canonical pathways. In addition, upstream regulator analysis was used to identify molecules upstream of the significantly DEGs that could potentially explain the observed expression differences between UA and placebo. Activation z-score (a measure of consistency between up/down gene regulation pattern and activation/inhibition pattern calculated by the IPA knowledgebase network) and P value of overlap (a measure of significance of enrichment of regulated genes in the dataset) were generated for each canonical pathway and upstream regulator.

Ex vivo analysis of mitochondrial parameters on human immune cells. For functional assays, PBMCs were cultivated in PBMC medium in the presence of UA (25 µM; Tocris; 6762) or DMSO control for the indicated time points. For the interrogation of mitochondrial parameters via flow cytometry, we used tetramethylrhodamine, methyl ester (TMRM; Thermo Fisher Scientific), LysoTracker red DND-99 (75 nM; Thermo Fisher Scientific), and MitoTracker Green (Thermo Fisher Scientific) according to the manufacturer's instructions.

To assess levels of Pink1 and Parkin, PBMCs were then stained with antibodies directed against Pink1 (sc-518052 PE; 1:100) and Parkin (sc-133167 AF647; 1:50) after incubation with UA or DMSO for the indicated time points. Permeabilization and fixation were performed using the BD transcription factor buffer set kit (BD Biosciences; 562574). The mtDNA/nuDNA ratio was calculated using the mean threshold cycle of ND1 for mitochondrial DNA and B2M for nuclear DNA, respectively. The primers used were as follows: ND1 Forward (5′-GAGCGATGGTGAGAGCTAAGGT-3′) and Reverse (5′-CCCTAAAACCCGCCACATCT-3′); B2M Forward (5′-TGCTGTCTCCATGTTTGATGTATCT-3′) and Reverse (5′-TCTCTGCTCC CCACCTCTAAGT-3′). Here, T cells were purified from PBMCs using the EasySep Human T Cell Kit (StemCell; 17951), followed by incubation in T cell medium in the presence of UA (25 µM) or DMSO for 48 h.

Statistics and reproducibility. All measurements were taken from distinct samples; no samples were measured repeatedly to generate data. No samples were excluded for the complete flow cytometry phenotyping constituting the primary end point of the present study. Samples for plasma cytokine analysis were chosen based on the availability of matched samples at baseline visit and after 28 days. Samples were excluded from analysis when cytokine level was not detectable. Samples from scRNA-seq were chosen to reflect a representative day 28 response after unblinding of the trial. According to the nature of this study, all other data collection and analysis were performed blind to the group allocation. Error bars correspond to 95% confidence interval and were plotted with GraphPad Prism (version 10). Repeated measures mixed effects models were performed for all comparisons here to test for significant differences of the respective variable between treatment groups by accounting for repeated measurements within the participants and by controlling for other covariates. Thereby, the participants were considered as random effects, and the variables treatment (group A versus group B), time (0 versus 28 days), the interaction between treatment and time, age, BMI, and the baseline values as fixed effects. P values depicted here represent the interaction between treatment and time. Model assumptions for the repeated measures mixed-effects model were assessed. Residuals were visually inspected for normality and homoscedasticity using diagnostic plots. All analyses were performed using SAS version 9.4 with SAS Enterprise Guide version 8.3. As one of our primary end points constitutes changes in mitochondrial function, this trial is powered to detect a difference in mitochondrial activity of immune cells between

treatment groups. Sample size estimates were based on statistical simulations by ref. 82 where a comprehensive literature review was performed to assess the range of effect size for 80% power when oxidative function of muscle cells was studied. According to these statistical simulations, 24 participants are considered sufficient for interventions with an expected 11% effect size. Likewise, the sample size chosen ($n = 50$) is comparable to a similar study in the literature[83] that focused on immune health and mitochondrial function.

Inclusion and ethics statement

All collaborators of this study have fulfilled the criteria for authorship required by Nature Portfolio journals and have been included as authors, as their participation was essential for the design and implementation of the study. Roles and responsibilities were agreed upon among collaborators ahead of the research. This work includes findings that are locally relevant, which have been determined in collaboration with local partners. This research was not severely restricted or prohibited in the setting of the researchers and does not result in stigmatization, incrimination, discrimination, or personal risk to participants. Local and regional research relevant to our study was taken into account in citations.

Reporting summary

Further information on research design is available in the Nature Portfolio Reporting Summary linked to this article.

Data availability

De-identified summary statistics in tabular form supporting the findings of this study are available from the corresponding author. Individual participant-level raw data containing confidential or identifiable patient information are subject to patient privacy and cannot be shared. Unique biological materials cannot be shared as they are restricted by participant consent. The scRNA-seq data generated in this study are publicly available in the National Center for Biotechnology Information Sequence Read Archive (SRA) under BioProject accession number PRJNA1169651.

References

1. Paludan, S. R., Pradeu, T., Masters, S. L. & Mogensen, T. H. Constitutive immune mechanisms: mediators of host defence and immune regulation. *Nat. Rev. Immunol.* **21**, 137–150 (2021).
2. Medzhitov, R. Origin and physiological roles of inflammation. *Nature* **454**, 428–435 (2008).
3. Denk, D. & Greten, F. R. Inflammation: the incubator of the tumor microenvironment. *Trends Cancer* **8**, 901–914 (2022).
4. Netea, M. G. et al. Defining trained immunity and its role in health and disease. *Nat. Rev. Immunol.* **20**, 375–388 (2020).
5. Hammarlund, E. et al. Duration of antiviral immunity after smallpox vaccination. *Nat. Med.* **9**, 1131–1137 (2003).
6. Wong, M. K. et al. COVID-19 mortality and progress toward vaccinating older adults - World Health Organization, Worldwide, 2020-2022. *MMWR Morb. Mortal. Wkly Rep.* **72**, 113–118 (2023).
7. Collier, D. A. et al. Age-related immune response heterogeneity to SARS-CoV-2 vaccine BNT162b2. *Nature* **596**, 417–422 (2021).
8. Goronzy, J. J. & Weyand, C. M. Understanding immunosenescence to improve responses to vaccines. *Nat. Immunol.* **14**, 428–436 (2013).
9. Mogilenko, D. A., Shchukina, I. & Artyomov, M. N. Immune ageing at single-cell resolution. *Nat. Rev. Immunol.* **22**, 484–498 (2022).
10. Franceschi, C., Garagnani, P., Parini, P., Giuliani, C. & Santoro, A. Inflammaging: a new immune-metabolic viewpoint for age-related diseases. *Nat. Rev. Endocrinol.* **14**, 576–590 (2018).
11. Furman, D. et al. Chronic inflammation in the etiology of disease across the life span. *Nat. Med.* **25**, 1822–1832 (2019).
12. Hotamisligil, G. S. Inflammation, metaflammation and immunometabolic disorders. *Nature* **542**, 177–185 (2017).
13. Park, E. J. et al. Dietary and genetic obesity promote liver inflammation and tumorigenesis by enhancing IL-6 and TNF expression. *Cell* **140**, 197–208 (2010).
14. Buck, M. D., Sowell, R. T., Kaech, S. M. & Pearce, E. L. Metabolic Instruction of Immunity. *Cell* **169**, 570–586 (2017).
15. Picca, A., Faitg, J., Auwerx, J., Ferrucci, L. & D'Amico, D. Mitophagy in human health, ageing and disease. *Nat. Metab.* **5**, 2047–2061 (2023).
16. López-Otín, C., Blasco, M. A., Partridge, L., Serrano, M. & Kroemer, G. Hallmarks of aging: an expanding universe. *Cell* **186**, 243–278 (2023).
17. Buck, M. D. et al. Mitochondrial dynamics controls T cell fate through metabolic programming. *Cell* **166**, 63–76 (2016).
18. Desdín-Micó, G. et al. T cells with dysfunctional mitochondria induce multimorbidity and premature senescence. *Science* **368**, 1371–1376 (2020).
19. Yu, Y.-R. et al. Disturbed mitochondrial dynamics in $CD8^+$ TILs reinforce T cell exhaustion. *Nat. Immunol.* **21**, 1540–1551 (2020).
20. Scharping, N. E. et al. The tumor microenvironment represses T cell mitochondrial biogenesis to drive intratumoral T cell metabolic insufficiency and dysfunction. *Immunity* **45**, 374–388 (2016).
21. Duggal, N. A, Pollock, R. D., Lazarus, N. R., Harridge, S. & Lord, J. M. Major features of immunesenescence, including reduced thymic output, are ameliorated by high levels of physical activity in adulthood. *Aging Cell* **17**, https://doi.org/10.1111/acel.12750 (2018)
22. Pietrocola, F. et al. Caloric restriction mimetics enhance anticancer immunosurveillance. *Cancer Cell* **30**, 147–160 (2016).
23. Borgoni, S., Kudryashova, K. S., Burka, K. & de Magalhães, J. P. Targeting immune dysfunction in aging. *Ageing Res. Rev.* **70**, 101410, https://doi.org/10.1016/j.arr.2021.101410 (2021).
24. D'Amico, D. et al. Impact of the natural compound urolithin A on health, disease, and aging. *Trends Mol. Med.* **27**, 687–699 (2021).
25. Andreux, P. A. et al. The mitophagy activator urolithin A is safe and induces a molecular signature of improved mitochondrial and cellular health in humans. *Nat. Metab.* **1**, 595–603 (2019).
26. Ryu, D. et al. Urolithin A induces mitophagy and prolongs lifespan in *C. elegans* and increases muscle function in rodents. *Nat. Med.* **22**, 879–888 (2016).
27. Singh, A. et al. Urolithin A improves muscle strength, exercise performance, and biomarkers of mitochondrial health in a randomized trial in middle-aged adults. *Cell Rep. Med.* **3**, 100633 (2022).
28. Liu, S. et al. Effect of urolithin A supplementation on muscle endurance and mitochondrial health in older adults: a randomized clinical trial. *JAMA Netw. Open* **5**, e2144279 (2022).
29. Denk, D. et al. Expansion of T memory stem cells with superior anti-tumor immunity by urolithin A-induced mitophagy. *Immunity* **55**, 2059–2073.e8 (2022).
30. Westera, L. et al. Closing the gap between T-cell life span estimates from stable isotope-labeling studies in mice and humans. *Blood* **122**, 2205–2212 (2013).
31. Alpert, A. et al. A clinically meaningful metric of immune age derived from high-dimensional longitudinal monitoring. *Nat. Med.* **25**, 487–495 (2019).
32. Terekhova, M. et al. Single-cell atlas of healthy human blood unveils age-related loss of $NKG2C^+GZMB^-CD8^+$ memory T cells and accumulation of type 2 memory T cells. *Immunity* **56**, 2836–2854.e9 (2023).
33. Fagnoni, F. F. et al. Shortage of circulating naive $CD8^+$ T cells provides new insights on immunodeficiency in aging. *Blood* **95**, 2860–2868 (2000).

34. Chiu, B.-C., Martin, B. E., Stolberg, V. R. & Chensue, S. W. Cutting edge: central memory CD8 T cells in aged mice are virtual memory cells. *J. Immunol.*) **191**, 5793–5796 (2013).
35. Wang, X. Q. et al. Spatial predictors of immunotherapy response in triple-negative breast cancer. *Nature* **621**, 868–876 (2023).
36. Mogilenko, D. A. et al. Comprehensive profiling of an aging immune system reveals clonal GZMK$^+$ CD8$^+$ T cells as conserved hallmark of inflammaging. *Immunity* **54**, 99–115.e12 (2021).
37. Scott, A. C. et al. TOX is a critical regulator of tumour-specific T cell differentiation. *Nature* **571**, 270–274 (2019).
38. Wang, X. et al. TOX promotes the exhaustion of antitumor CD8$^+$ T cells by preventing PD1 degradation in hepatocellular carcinoma. *J. Hepatol.* **71**, 731–741 (2019).
39. Argüello, R. J. et al. SCENITH: a flow cytometry-based method to functionally profile energy metabolism with single-cell resolution. *Cell Metab.* **32**, 1063–1075.e7 (2020).
40. Chang, C.-H. et al. Posttranscriptional control of T cell effector function by aerobic glycolysis. *Cell* **153**, 1239–1251 (2013).
41. Ma, E. H. et al. Metabolic profiling using stable isotope tracing reveals distinct patterns of glucose utilization by physiologically activated CD8$^+$ T cells. *Immunity* **51**, 856–870.e5 (2019).
42. van der Windt, G. J. et al. Mitochondrial respiratory capacity is a critical regulator of CD8$^+$ T cell memory development. *Immunity* **36**, 68–78 (2011).
43. Schulte-Schrepping, J. et al. Severe COVID-19 is marked by a dysregulated myeloid cell compartment. *Cell* **182**, 1419–1440.e23 (2020).
44. Rambold, A. S. & Pearce, E. L. Mitochondrial dynamics at the interface of immune cell metabolism and function. *Trends Immunol.* **39**, 6–18 (2018).
45. Finck, B. N. & Kelly, D. P. PGC-1 coactivators: inducible regulators of energy metabolism in health and disease. *J. Clin. Invest.* **116**, 615–622 (2006).
46. Perl, A., Gergely, P., Nagy, G., Koncz, A. & Banki, K. Mitochondrial hyperpolarization: a checkpoint of T-cell life, death and autoimmunity. *Trends Immunol.* **25**, 360–367 (2004).
47. Mittelbrunn, M. & Kroemer, G. Hallmarks of T cell aging. *Nat. Immunol.* **22**, 687–698 (2021).
48. Hao, Y. et al. Integrated analysis of multimodal single-cell data. *Cell* **184**, 3573–3587.e29 (2021).
49. Chen, J. et al. NR4A transcription factors limit CAR T cell function in solid tumours. *Nature* **567**, 530–534 (2019).
50. Globig, A.-M. et al. The β1-adrenergic receptor links sympathetic nerves to T cell exhaustion. *Nature* **622**, 383–392 (2023).
51. Tinoco, R., Alcalde, V., Yang, Y., Sauer, K. & Zuniga, E. I. Cell-intrinsic transforming growth factor-beta signaling mediates virus-specific CD8$^+$ T cell deletion and viral persistence in vivo. *Immunity* **31**, 145–157 (2009).
52. Jackson, C. M., et al. The cytokine Meteorin-like inhibits anti-tumor CD8$^+$ T cell responses by disrupting mitochondrial function. *Immunity* https://doi.org/10.1016/j.immuni.2024.07.003 (2024).
53. Kuleshov, M. V. et al. Enrichr: a comprehensive gene set enrichment analysis web server 2016 update. *Nucleic Acids Res.* **44**, W90–W97 (2016).
54. Wu, V. H. et al. The GPCR-Gαs-PKA signaling axis promotes T cell dysfunction and cancer immunotherapy failure. *Nat. Immunol.* **24**, 1318–1330 (2023).
55. Man, K. et al. Transcription factor IRF4 promotes CD8$^+$ T cell exhaustion and limits the development of memory-like T cells during chronic infection. *Immunity* **47**, 1129–1141.e5 (2017).
56. Yang, C. et al. Heterogeneity of human bone marrow and blood natural killer cells defined by single-cell transcriptome. *Nat. Commun.* **10**, 3931 (2019).
57. Tullai, J. W. et al. Immediate-early and delayed primary response genes are distinct in function and genomic architecture. *J. Biol. Chem.* **282**, 23981–23995 (2007).
58. Rebuffet, L. et al. High-dimensional single-cell analysis of human natural killer cell heterogeneity. *Nat. Immunol.* **25**, 1474–1488 (2024).
59. Covarrubias, A. J. et al. Senescent cells promote tissue NAD$^+$ decline during ageing via the activation of CD38$^+$ macrophages. *Nat. Metab.* **2**, 1265–1283 (2020).
60. Pong Ng, H., Kim, G.-D., Ricky Chan, E., Dunwoodie, S. L. & Mahabeleshwar, G. H. CITED2 limits pathogenic inflammatory gene programs in myeloid cells. *FASEB J.* **34**, 12100–12113 (2020).
61. Villar, J. et al. ETV3 and ETV6 enable monocyte differentiation into dendritic cells by repressing macrophage fate commitment. *Nat. Immunol.* **24**, 84–95 (2023).
62. Morgan, D. & Tergaonkar, V. Unraveling B cell trajectories at single cell resolution. *Trends Immunol.* **43**, 210–229 (2022).
63. *Ageing and Health* (World Health Organization, 2022); https://www.who.int/news-room/fact-sheets/detail/ageing-and-health
64. Takahashi, T. et al. Sex differences in immune responses that underlie COVID-19 disease outcomes. *Nature* **588**, 315–320 (2020).
65. Yin, K. et al. Long COVID manifests with T cell dysregulation, inflammation and an uncoordinated adaptive immune response to SARS-CoV-2. *Nat. Immunol.* **25**, 218–225 (2024).
66. Fane, M. & Weeraratna, A. T. How the ageing microenvironment influences tumour progression. *Nat. Rev. Cancer* **20**, 89–106 (2020).
67. Carrasco, E. et al. The role of T cells in age-related diseases. *Nat. Rev. Immunol.* **22**, 97–111 (2022).
68. Biasco, L. et al. In vivo tracking of T cells in humans unveils decade-long survival and activity of genetically modified T memory stem cells. *Sci. Transl. Med.* **7**, 273ra13 (2015).
69. Gattinoni, L., Speiser, D. E., Lichterfeld, M. & Bonini, C. T memory stem cells in health and disease. *Nat. Med.* **23**, 18–27 (2017).
70. Boakye, Y. D., Groyer, L. & Heiss, E. H. An increased autophagic flux contributes to the anti-inflammatory potential of urolithin A in macrophages. *Biochim. Biophys. Acta Gen. Subj.* **1862**, 61–70 (2018).
71. Tur, J. et al. Mitofusin 2 in macrophages links mitochondrial ROS production, cytokine release, phagocytosis, autophagy, and bactericidal activity. *Cell Rep.* **32**, 108079 (2020).
72. Ferrara, R. et al. Circulating T-cell immunosenescence in patients with advanced non-small cell lung cancer treated with single-agent PD-1/PD-L1 inhibitors or platinum-based chemotherapy. *Clin. Cancer Res.* **27**, 492–503 (2021).
73. Bengsch, B. et al. Bioenergetic insufficiencies due to metabolic alterations regulated by the inhibitory receptor PD-1 are an early driver of CD8(+) T cell exhaustion. *Immunity* **45**, 358–373 (2016).
74. Simula, L. et al. Mitochondrial metabolism sustains CD8$^+$ T cell migration for an efficient infiltration into solid tumors. *Nat. Commun.* **15**, 2203 (2024).
75. Singh, A. et al. Direct supplementation with urolithin A overcomes limitations of dietary exposure and gut microbiome variability in healthy adults to achieve consistent levels across the population. *Eur. J. Clin. Nutr.* **76**, 297–308 (2022).
76. Hao, Y. et al. Dictionary learning for integrative, multimodal and scalable single-cell analysis. *Nat. Biotechnol.* **42**, 293–304 (2024).
77. Butler, A., Hoffman, P., Smibert, P., Papalexi, E. & Satija, R. Integrating single-cell transcriptomic data across different conditions, technologies, and species. *Nat. Biotechnol.* **36**, 411–420 (2018).
78. Satija, R., Farrell, J. A., Gennert, D., Schier, A. F. & Regev, A. Spatial reconstruction of single-cell gene expression data. *Nat. Biotechnol.* **33**, 495–502 (2015).

79. McGinnis, C. S., Murrow, L. M. & Gartner, Z. J. DoubletFinder: doublet detection in single-cell RNA sequencing data using artificial nearest neighbors. *Cell Syst.* **8**, 329–337.e4 (2019).
80. Korsunsky, I. et al. Fast, sensitive and accurate integration of single-cell data with Harmony. *Nat. Methods* **16**, 1289–1296 (2019).
81. Yu, G., Wang, L.-G., Han, Y. & He, Q.-Y. clusterProfiler: an R package for comparing biological themes among gene clusters. *OMICS* **16**, 284–287 (2012).
82. Jacques, M. et al. Mitochondrial respiration variability and simulations in human skeletal muscle: the Gene SMART study. *FASEB J.* **34**, 2978–2986 (2020).
83. Zhou, B. et al. Boosting NAD level suppresses inflammatory activation of PBMCs in heart failure. *J. Clin. Invest.* **130**, 6054–6063 (2020).

Acknowledgements

We would like to thank the volunteers for their participation in the study and the study unit staff of the Medical Department I of the University Hospital Frankfurt (C. Back, H. Bolotin, K. Lorenz-Pabijan, S. Flebbe, C. Bott). This trial was supported by the Clinical Trial Center Network of the Universitäres Centrum für Tumorerkrankungen (UCT) Frankfurt. We thank S. Hehn of the UCT Frankfurt for eCRF support. We thank E. Rudolf and K. Mohs for expert technical assistance. P. Ziegler provided critical assistance recruiting participants for this trial. UA (Mitopure) and study funds were provided by Amazentis SA. The funders co-designed this investigator-initiated trial but had no role in data collection, analysis, decision to publish, or preparation of the manuscript. D. Denk was supported by the Mildred-Scheel Nachwuchszentrum Frankfurt funded by the German Cancer Aid and the Walter Benjamin Program Post-Doctoral Fellowship by the Deutsche Forschungsgemeinschaft (DE 4233/1-1; project number 548709808). Work in the lab of F.R.G. is supported by institutional funds from the Georg-Speyer-Haus, by the LOEWE Center Frankfurt Cancer Institute funded by the Hessen State Ministry for Higher Education, Research and the Arts (III L 5 - 519/03/03.001 - (0015)), Deutsche Forschungsgemeinschaft (SFB1292-Project ID: 318346496-TP16; SFB1479-Project ID: 441891347-P02; GRK2336) the German Federal Ministry of Education and Research (BMBF; 01KD2206Q/SATURN3), and the European Research Council (Advanced Grant PLASTICAN-101021078). The Institute for Tumor Biology and Experimental Therapy, Georg-Speyer-Haus is funded jointly by the German Federal Ministry of Health and the Ministry of Higher Education, Research and the Arts of the State of Hessen (HMWK).

Author contributions

Conceptualization: D. Denk, A.S. and F.R.G.; methodology: D. Denk, H.G.K. and R.J.A.; investigation: D. Denk, H.G.K., D. D'Amico, L.A.-B., J.R., J.F., J.M.G., C.S., R.T. and R.K.; resources: E.V., C.R., K.S., S.Z., V.N., S.L. and F.R.G.; writing—original draft: D. Denk and F.R.G.; visualization: D. Denk and F.R.G.; supervision and funding acquisition: C.R. and F.R.G.

Competing interests

A.S., D. D'Amico and J.F. are employees, and C.R. is president and delegate of the board of Amazentis SA, which funded this clinical study and provided the investigational product (Mitopure). F.R.G. has received consulting fees from Amazentis. D. Denk has received travel compensation from Amazentis and AbbVie. There are restrictions to the commercial use of SCENITH due to a pending patent application (PCT/EP2020/WO2020212362A1 to R.J.A.). The remaining authors declare no competing interests related to this study.

Additional information

Extended data is available for this paper at https://doi.org/10.1038/s43587-025-00996-x.

Supplementary information The online version contains supplementary material available at https://doi.org/10.1038/s43587-025-00996-x.

Correspondence and requests for materials should be addressed to Florian R. Greten.

Peer review information *Nature Aging* thanks Vilhelm Bohr and the other, anonymous, reviewer(s) for their contribution to the peer review of this work.

Reprints and permissions information is available at www.nature.com/reprints.

Publisher's note Springer Nature remains neutral with regard to jurisdictional claims in published maps and institutional affiliations.

Dominic Denk[1,2,3], Anurag Singh[4], Herbert G. Kasler[5], Davide D'Amico[4], Julia Rey[5], Lucía Alcober-Boquet[2], Johanna M. Gorol[1], Christoph Steup[1,2], Ritesh Tiwari[5], Ryan Kwok[6], Rafael J. Argüello[7], Julie Faitg[4], Kathrin Sprinzl[2], Stefan Zeuzem[2,8], Valentina Nekljudova[5], Sibylle Loibl[5], Eric Verdin[6], Chris Rinsch[4] & Florian R. Greten[1,3,8]

[1]Institute for Tumor Biology and Experimental Therapy, Georg-Speyer-Haus, Frankfurt am Main, Germany. [2]Department of Medicine I, University Hospital Frankfurt, Goethe University Frankfurt, Frankfurt am Main, Germany. [3]Frankfurt Cancer Institute, Goethe University Frankfurt, Frankfurt am Main, Germany. [4]Amazentis SA, Lausanne, Switzerland. [5]GBG c/o GBG Forschungs GmbH, Neu-Isenburg, Germany. [6]Buck Institute for Research on Aging, Novato, CA, USA. [7]Aix Marseille Univ, CNRS, INSERM, CIML, Centre d'Immunologie de Marseille-Luminy, Marseille, France. [8]German Cancer Consortium (DKTK) and German Cancer Research Center (DKFZ), Heidelberg, Germany. e-mail: greten@gsh.uni-frankfurt.de

https://doi.org/10.1038/s43587-025-00996-x

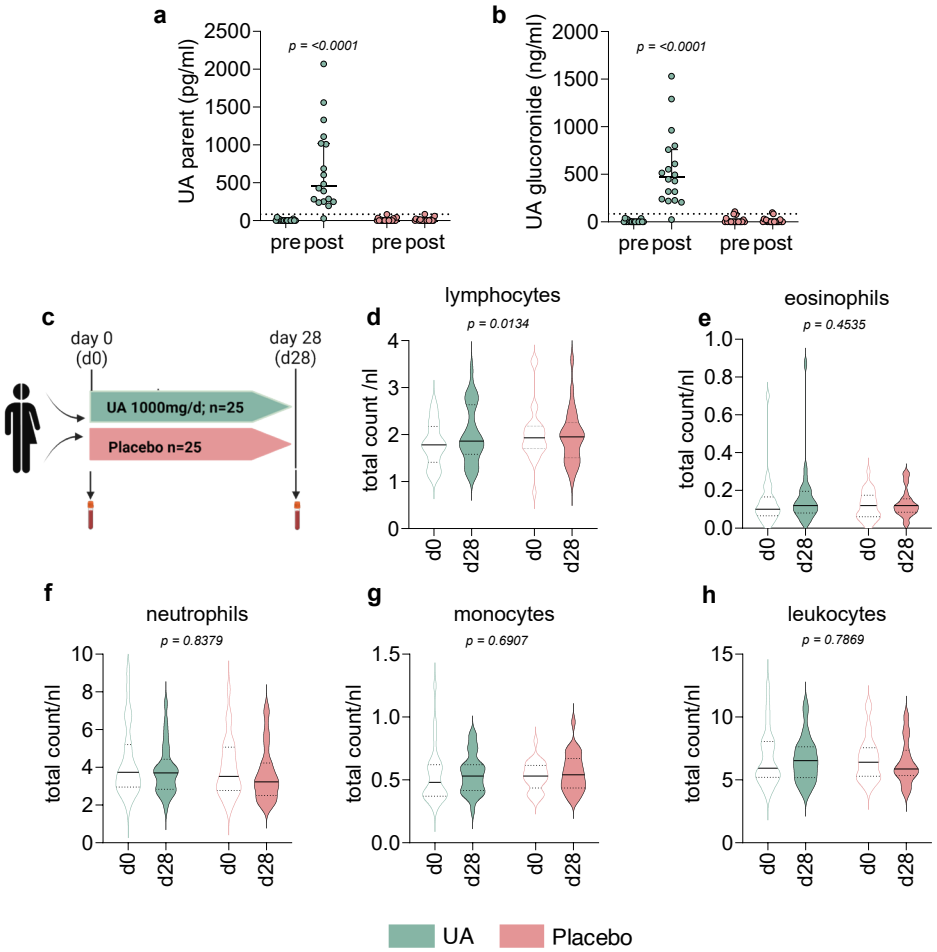

Extended Data Fig. 1 | Bioavailability and clinical hemocytometry. **(a-b)** Bioavailability data. Plasma levels of UA-parent (**b**) and UA glucuronide (**c**) before and after intake of UA and placebo, respectively. N = 20 per group. Data are median + 95% CI, p-value depicts treatment effect as assessed by a two-sided repeated measures mixed-effect model. **(c)** Clinical trial overview. Fifty (n = 50) healthy participants were randomized (1:1) to either placebo softgels or 1000 mg UA per day. Blood was drawn at baseline and 28 days to profile circulating immune cells. **(d)** Total lymphocyte count of participants in the UA intervention arm (left panel) and placebo (right panel) intervention arm. Changes from baseline measurement (day 0; d0) and last study visit (day 28; d28) are shown. N = 25 per violin plot. P-value for treatment effect was calculated by a repeated measures mixed-effect model, depicting the treatment-by-time effect. **(e)** Total eosinophil count of participants in the UA intervention arm (left panel) and placebo (right panel) intervention arm. Changes from baseline measurement (d0) and last study visit (d28) are shown. P-value for treatment effect was calculated by a repeated measures mixed-effect model, depicting the treatment-by-time effect. **(f-g)** Total count of neutrophils, monocytes and leukocytes in the UA group and the placebo intervention group. Violin plots for values at baseline visit and final study visit (d28) are shown. N = 25 per violin plot. All comparisons are not significant. P-value for treatment effect was calculated by a repeated measures mixed-effect model, depicting the treatment-by-time effect. All statistical tests were two-sided. No adjustments for multiple comparisons were made.

https://doi.org/10.1038/s43587-025-00996-x

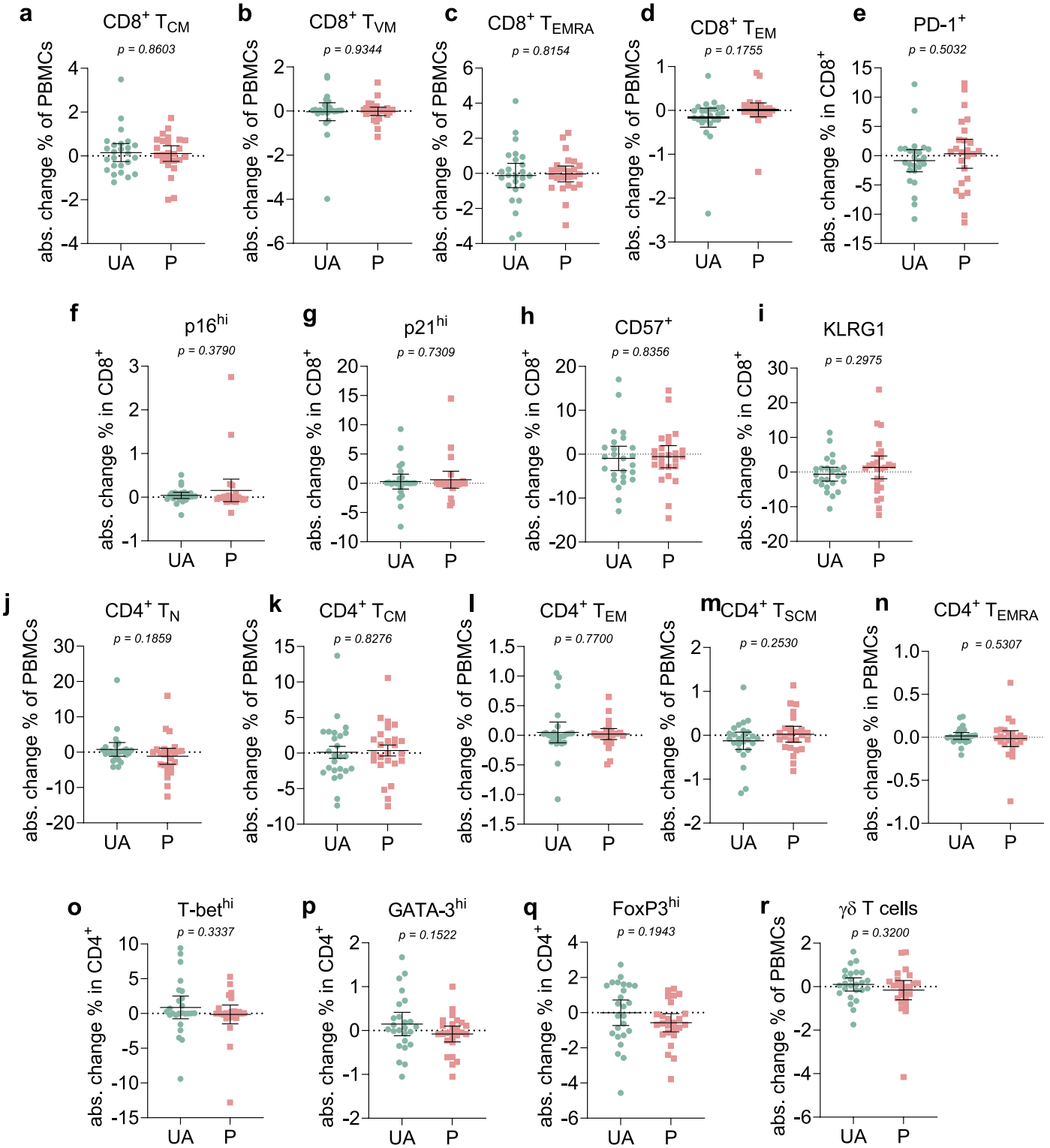

Extended Data Fig. 2 | Unaltered T cell subpopulations. (a-d) Distribution of $CD8^+$ subsets within PBCMs depicted as absolute change in percentage of PBMCs after 28 days of UA intake (U) or placebo (P). Data are mean ± 95% CI, n = 25 per group as assessed by spectral flow cytometry. **(e)** Changes in $CD8^+$ expression of PD-1, depicted as absolute change in percentage points. Data refers to changes after 28 days of UA intake (U) or placebo (P). Data are mean ± 95% CI, n = 25 per group as assessed by spectral flow cytometry. **(f-i)** Changes in $CD8^+$ expression of CD57 (f), KLRG1 (g), p16 (h) and p21 (i), depicted as absolute change in percentage points. Data refers to changes after 28 days of UA intake (U) or placebo (P). Data are mean ± 95% CI, n = 25 per group as assessed by spectral flow cytometry. **(j-n)** Distribution of $CD4^+$ subsets depicted as absolute change in percentage of PBMCs after 28 days of UA intake (U) or placebo (P). Shows data of $CD4^+$ T_N (j), $CD4^+$ T_{CM} (k) $CD4^+$ T_{EM} (l), $CD4^+$ T_{SCM} (m) and $CD4^+$ T_{EMRA} (n) subsets. Data are mean ± 95% CI, n = 25 per group as assessed by spectral flow cytometry. **(o-q)** Changes in T-bet^{hi}, GATA-3^{hi}, and FoxP3^{hi} $CD4^+$ cells depicted as absolute change in percentage points of total CD4+ after 28 days of UA intake (U) or placebo (P). Data are mean ± 95% CI, n = 25 per group as assessed by spectral flow cytometry. **(r)** Changes of γδ $CD3^+$ cells depicted as absolute change in percentage of PBMCs after 28 days of UA intake (U) or placebo (P). Data are mean ± 95% CI, n = 25 per group as assessed by spectral flow cytometry. For all subpanels, p-values for treatment effects were calculated by a two-dided repeated measures mixed-effect model using the percentage of the depicted population at timepoints d = 0 and d = 28 (treatment-by-time effect). No adjustments were multiple comparisons were made.

https://doi.org/10.1038/s43587-025-00996-x

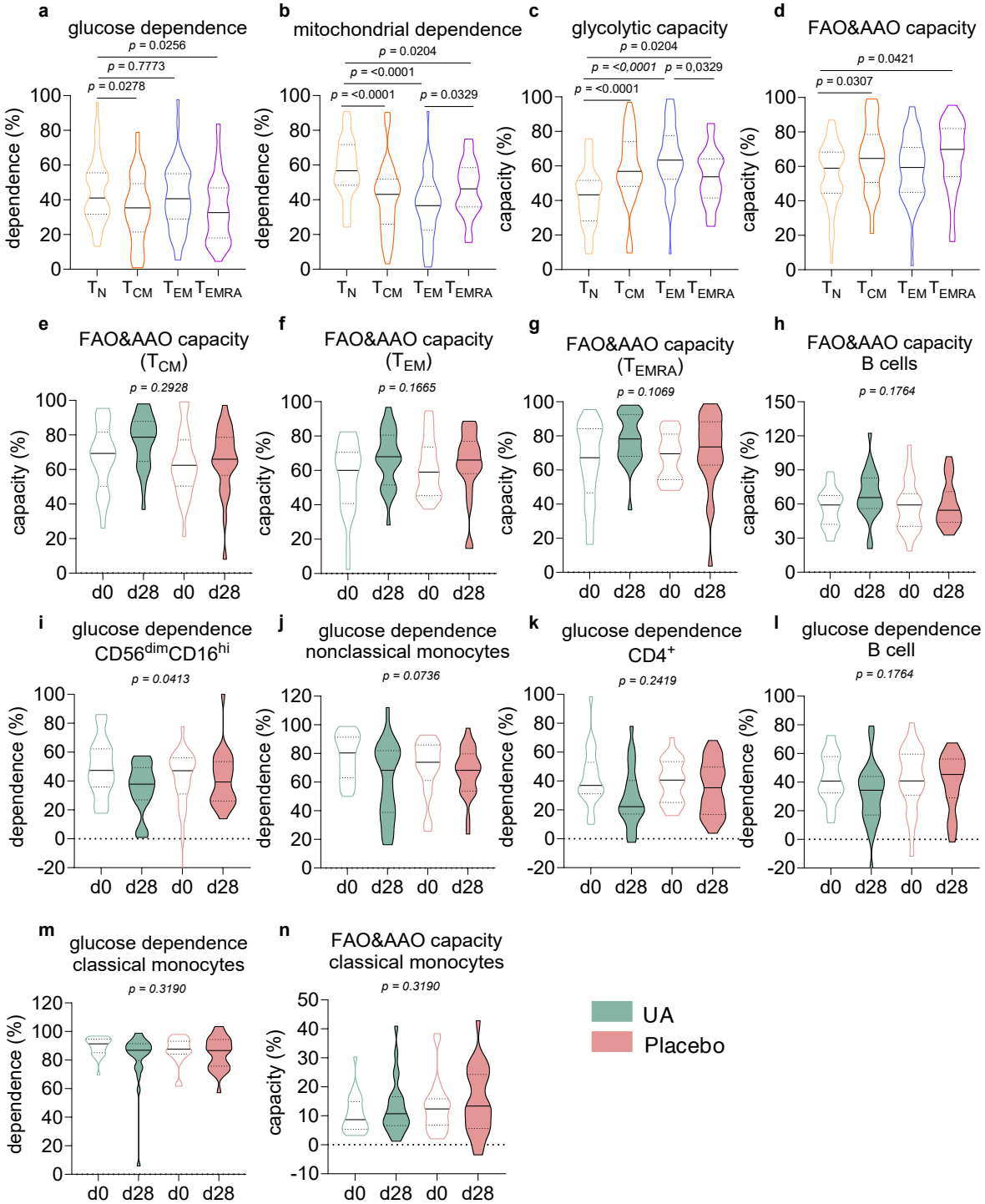

Extended Data Fig. 3 | Effect of UA on immune metabolism. (a-d) Metabolic profiling of $CD8^+$ subpopulations using Scenith. Truncated violin plots of glucose dependence (**a**), mitochondrial dependence (**b**), glycolytic capacity (**c**), and fatty acid and amino acid oxidation capacity (FAO&AAO capacity) are shown. Data derived from T_N, T_{CM}, T_{EM} and T_{EMRA} subpopulations from n = 50 participants at baseline (d0). Depicts mean (solid line) and 25th/75th quartiles (dotted lines), n = 25 per group. Exact p-values are shown, calculated by ordinary one-way ANOVA with Tukey's multiple comparison's test. **(e-h)** Truncated violin plots of fatty acid and amino acid oxidation (FAO&AAO) from several immune populations as assessed by SCENITH. Data from $CD8^+$ T_{CM} (e), $CD8^+$ T_{EM} (f), $CD8^+$ T_{EMRA} (**g**) and B cells (**h**) are shown from UA and placebo treated participants at baseline (d0) and after the 28-day supplementation period (d28). Mean (solid line) and 25th/75th quartiles (dotted lines) are depicted. N = 25 per group. **(i-l)** Truncated violin plots depicting glucose dependence from several immune populations as assessed by Scenith. Data from NK cells (**i**), non classical monocytes (**j**), $CD4^+$ cells (**k**), and B cells (l) are shown from UA and placebo treated participants at baseline (d0) and after the 28-day supplementation period (d28). Depicts mean (solid line) and 25th/75th quartiles (dotted lines), n = 25 per group. **(m-n)** Truncated violin plots depicting glucose dependence and fatty acid and amino acid oxidation (FAO&AAO) capacity from classical monocytes as assessed by Scenith. Data from UA and placebo treated participants at baseline (d0) and after the 28-day supplementation period (d28). Depicts mean (solid line) and 25th/75th quartiles (dotted lines), n = 25 per group. P-values for treatment effects in e-h were calculated by a two-sided repeated measures mixed-effect model using the percentage of the depicted population at timepoints d = 0 and d = 28 (treatment-by-time effect). No adjustments for multiple comparisons were made.

https://doi.org/10.1038/s43587-025-00996-x

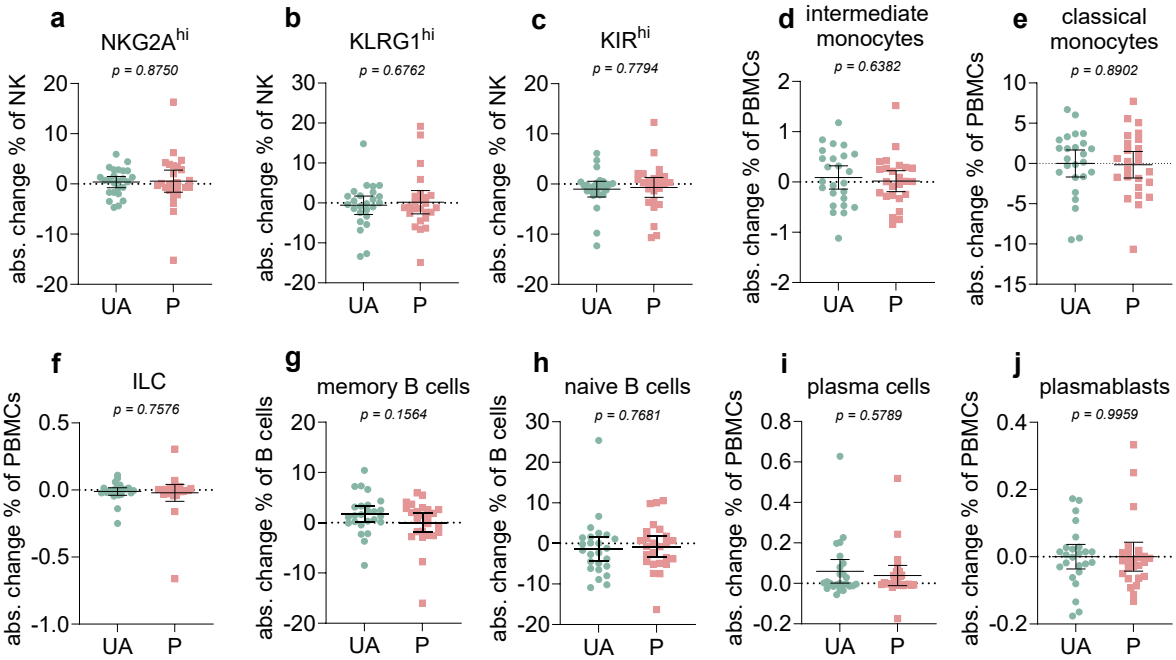

Extended Data Fig. 4 | Effect of UA on peripheral immune populations. (**a-c**) Tertiary markers on $CD56^{lo}CD16^{hi}$ NK cells. Changes in expression of NKG2A (**c**), KIR (**d**) and KLRG1 (**e**) are depicted as absolute change in percentage points. Data refers to changes after 28 days of UA intake (U) or placebo (P). Data are mean ± 95% CI, n = 25 per group as assessed by spectral flow cytometry. P-values for treatment effects were calculated by a repeated measures mixed-effect model using the percentage of the depicted population at timepoints d = 0 and d = 28. **(d)** Absolute change of intermediate monocytes within PBMCs after 28 days. Data are mean ± 95% CI, n = 25 per group. P-values for treatment effects were calculated by a repeated measures mixed-effect model using the percentage of the depicted population at timepoints d = 0 and d = 28. **(e)** Absolute change of classical monocytes within PBMCs after 28 days. Data are mean ± 95% CI, n = 25 per group, P-values for treatment effects were calculated by a repeated measures mixed-effect model using the percentage of the depicted population at timepoints d = 0 and d = 28. **(f)** Absolute change in percentage ILCs (f) in PBMCs. Data are mean ± 95% CI, n = 25 per group as assessed by spectral flow cytometry. P-values for treatment effects were calculated by a repeated measures mixed-effect model using the percentage of the depicted population at timepoints d = 0 and d = 28. **(g-h)** Changes within the memory B cell (g) and naïve B cell (h) population depicted as absolute change in percentage points. Data refers to changes after 28 days of UA intake (U) or placebo (P). Data are mean ± 95% CI, n = 25 per group as assessed by spectral flow cytometry. P-values for treatment effects were calculated by a repeated measures mixed-effect model using the percentage of the depicted population at timepoints d = 0 and d = 28. **(i-j)** Changes of plasma cells (i) and plasma blasts (j) cells depicted as absolute change in percentage of PBMCs after 28 days of UA intake (U) or placebo (P). Data are mean ± 95% CI, n = 25 per group as assessed by spectral flow cytometry. P-values for treatment effects were calculated by a repeated measures mixed-effect model using the percentage of the depicted population at timepoints d = 0 and d = 28. All statistical tests were two-sided. No adjustments for multiple comparisons were made.

https://doi.org/10.1038/s43587-025-00996-x

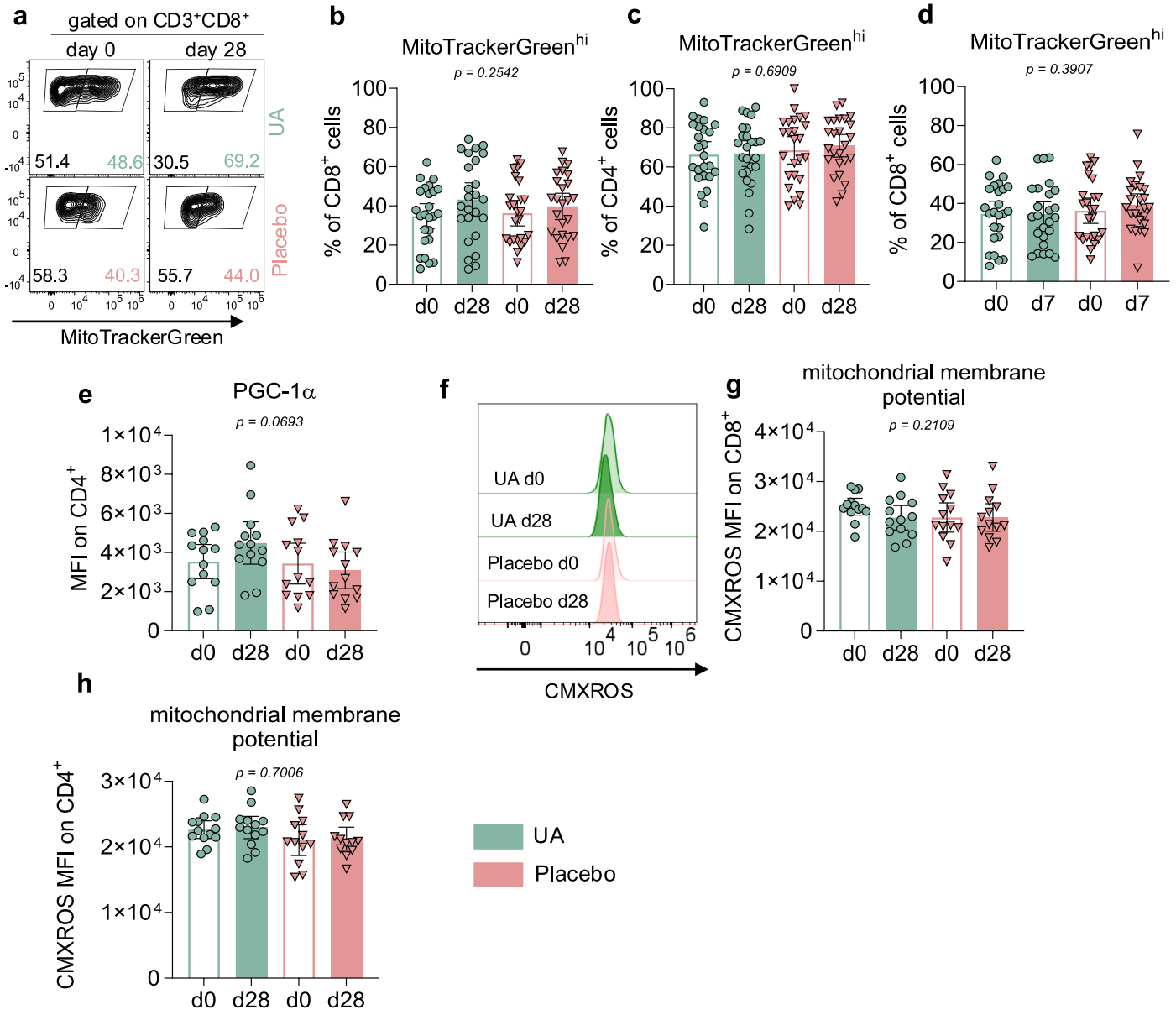

Extended Data Fig. 5 | Effect of UA on mitochondrial parameters. **(a)** Representative gating strategy to identify MitotrackerGreen^{hi} cells within the CD3$^+$CD8$^+$ population at baseline (d0) and after 28 days (d28) of UA and placebo supplementation, respectively. **(b)** Percentage of MitotrackerGreen^{hi} cells within CD8$^+$ cells as identified in (a). Data are mean ± 95% CI, n = 25 per group. P-value for treatment effect was calculated by a repeated measures mixed-effect model. **(c)** Percentage of MitotrackerGreen^{hi} cells within CD4$^+$ cells. Data are mean ± 95% CI, n = 25 per group. P-value for treatment effect was calculated by a repeated measures mixed-effect model. **(d)** Percentage of MitotrackerGreen^{hi} cells within CD8$^+$ cells after seven days of either UA or placebo treatment. Data are mean ± 95% CI, n = 25 per group. P-value for treatment effect was calculated by a repeated measures mixed-effect model. **(e)** Expression of PGC-1α in CD4$^+$ cells before (d0) and after (d28) UA and placebo supplementation, respectively. Assessed by flow cytometry, data shown as MFI. Data are mean ± 95% CI, n = 13 per group. P-value for treatment effects were calculated by a repeated measures mixed-effect model. **(f-h)** Mitochondrial membrane potential (MMP) in CD8$^+$ (**g**) and and CD4$^+$ cells (**h**) before (d0) and after (d28) UA and placebo supplementation, respectively. Assessed by MitotrackerCMXROS staining, data shown as MFI. Representative histograms are shown in (**f**). Data are mean ± 95% CI, n = 12/13 per group. P-value for treatment effects were calculated by a repeated measures mixed-effect model. All statistical tests were two-sided. No adjustments for multiple comparisons were made.

https://doi.org/10.1038/s43587-025-00996-x

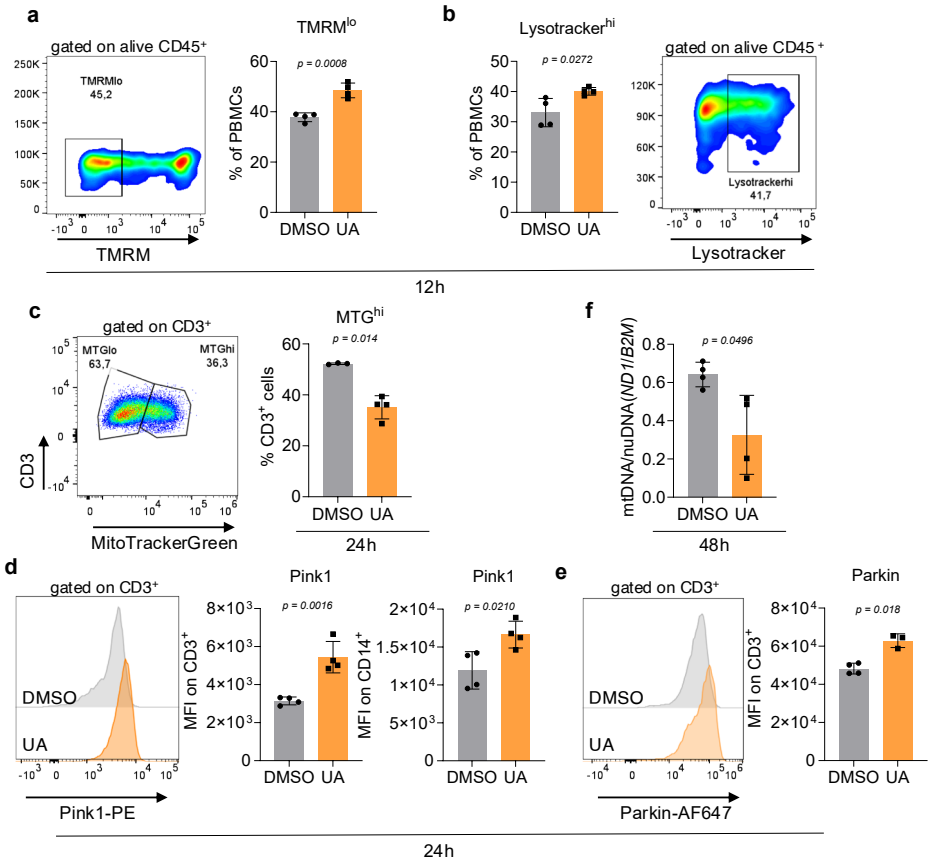

Extended Data Fig. 6 | UA elicits mitophagy rapidly ex vivo. (a-b) Flow cytometry analysis of mitochondrial membrane potential in human CD45$^+$ cells treated *ex vivo* with DMSO control or 25 µM Urolithin A (UA) for 12 h. Percentage of TMRM^{lo} cells is shown. Data are mean ± SD, n = 4 per group. P- value by unpaired, two-tailed t-test. Depicts one out of two independent experiments. **(b)** Flow cytometry analysis of lysosome formation potential in human CD45$^+$ cells, treated *ex vivo* with DMSO control or 25 µM Urolithin A (UA) for 12 h. Percentage of Lysotracker^{hi} cells is shown. Data are mean ± SD, n = 4 per group. P- value by unpaired, two-tailed t-test. Depicts one out of two independent experiments. **(c)** Flow cytometry analysis mitochondrial mass potential in human CD3$^+$ cells, treated with DMSO control or 25 µM Urolithin A (UA) for 24 h. Percentage of MitoTrackerGreen^{lo} cells is shown. Data are mean ± SD, n = 4 per group. P- value by unpaired, two-tailed t-test. Depicts one out of two independent experiments. **(d)** Flow cytometry analysis of Pink1 protein levels. Human PBMCs were treated with 25 µM UA or DMSO control for 24 h. MFIs of CD3$^+$ and CD14$^+$ cells are shown. Data are mean ± SD, n = 4 per group. P- value by unpaired, two-tailed t-test. Depicts one out of two independent experiments. **(e)** Flow cytometry analysis of Parkin protein levels. Human PBMCs were treated with 25 µM UA or DMSO control for 24 h. MFIs of CD3$^+$ cells are shown. Data are mean ± SD, n = 3/4 per group. P- value by unpaired, two-tailed t-test. Depicts one out of two independent experiments. **(f)** Ratio of nuclear DNA to mitochondrial DNA in human CD3$^+$ cells after 48 h in the presence of UA (25 µM) or placebo. Data are mean ± SD, n = 3/4 per group. P- value by unpaired, two-tailed t-test with Welsh's correction. Depicts one out of two independent experiments.

https://doi.org/10.1038/s43587-025-00996-x

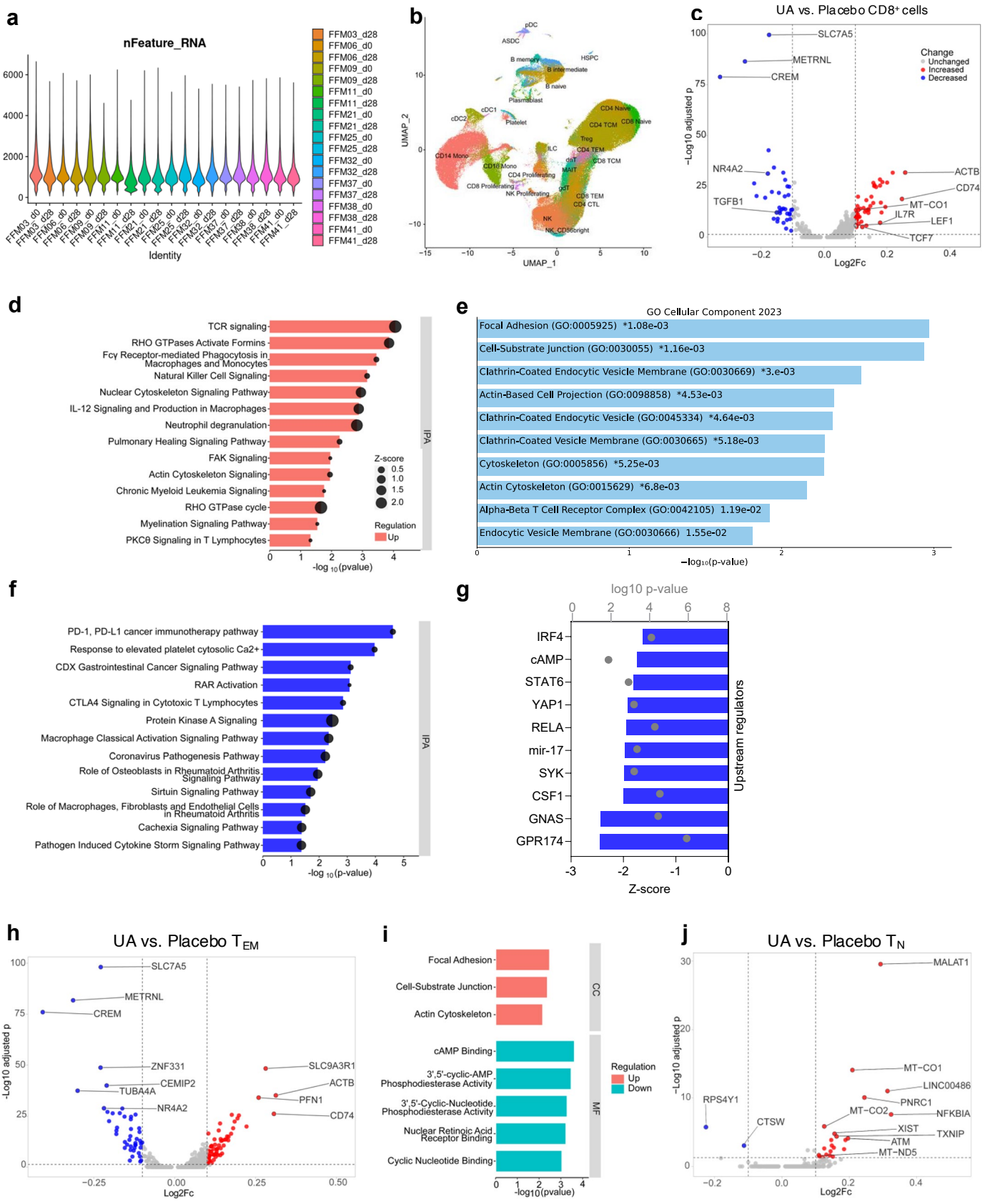

Extended Data Fig. 7 | See next page for caption.

https://doi.org/10.1038/s43587-025-00996-x

Extended Data Fig. 7 | Single cell RNA sequencing reveals UA-mediated transcriptional alterations in T cells. (**a**) Violin plot displaying the average number of genes per cell. Data from every analyzed sample shown (n = 5 per treatment, matched d0 and d28 samples). (**b**) Unsupervised Uniform Manifold Approximation and Projection (UMAP) visualization of PBMCs with clusters identified by unsupervised hierarchical clustering. (**c**) Volcano plot of differentially expressed genes within $CD8^+$ cells in UA treated participants vs. placebo after the 28-day intervention period. Red dots represent genes expressed at higher levels in $CD8^+$ cells from UA-treated participants, while blue dots represent genes with lower expression levels compared to baseline visit. Genes with log2fc ≥ 0.1 and $p < 0.05$ were considered significant. (**d**) Ingenuity pathway Analysis (IPA) of $CD8^+$ cells, displaying activated canonical pathways in $CD8^+$ cells of UA treated participants. Ranking was performed based on -log10 p-value. Z-scores of affected pathways are shown. (**e**) Gene Ontology (GO) term enrichment analysis of $CD8^+$ cells after 28 days of UA intake using the web-based tool Enrichr. Top upregulated terms and suppressed terms among the "cellular components" domain are shown. Ranking was performed based on adjusted -log10 p-value. Genes with log2fc ≥ 0.1 and $p < 0.05$ were considered for input. (**f**) Ingenuity pathway Analysis (IPA) of $CD8^+$ cells, displaying inhibited canonical pathways in $CD8^+$ cells of UA treated participants. Ranking was performed based on -log10 p-value. Z-scores of affected pathways are shown. (**g**) Biological upstream regulator analysis of CD8+ cells from UA-treated participants after the intervention period. Predicted inhibited upstream regulators as established by IPA are shown, ranked based on -log10 p-value. Respective inhibition z-scores are shown. (**h**) Volcano plot of differentially expressed genes within $CD8^+ T_{EM}$ in UA treated participants vs. placebo after the 28-day intervention period. Red dots represent genes expressed at higher levels in T_{EM} from UA-treated participants, while blue dots represent genes with lower expression levels. Genes with log2fc ≥ 0.1 and $p < 0.05$ were considered significant. (**i**) Gene Ontology (GO) term enrichment analysis of $CD8^+ T_{EM}$ cells after UA intake. Top upregulated terms and suppressed terms among CC (cellular components) and MF (molecular functions) domains are shown. Ranking was performed on adjusted -log10 p-value. Genes with log2fc ≥ 0.1 and $p < 0.05$ were considered for input. (**j**) Volcano plot of differentially expressed genes within CD8 + T_N in UA treated participants vs. placebo after the 28-day intervention period. Red dots represent genes expressed at higher levels in T_N from UA-treated participants, while blue dots represent genes with lower expression levels. Genes with log2fc ≥ 0.1 and $p < 0.05$ were considered significant.

https://doi.org/10.1038/s43587-025-00996-x

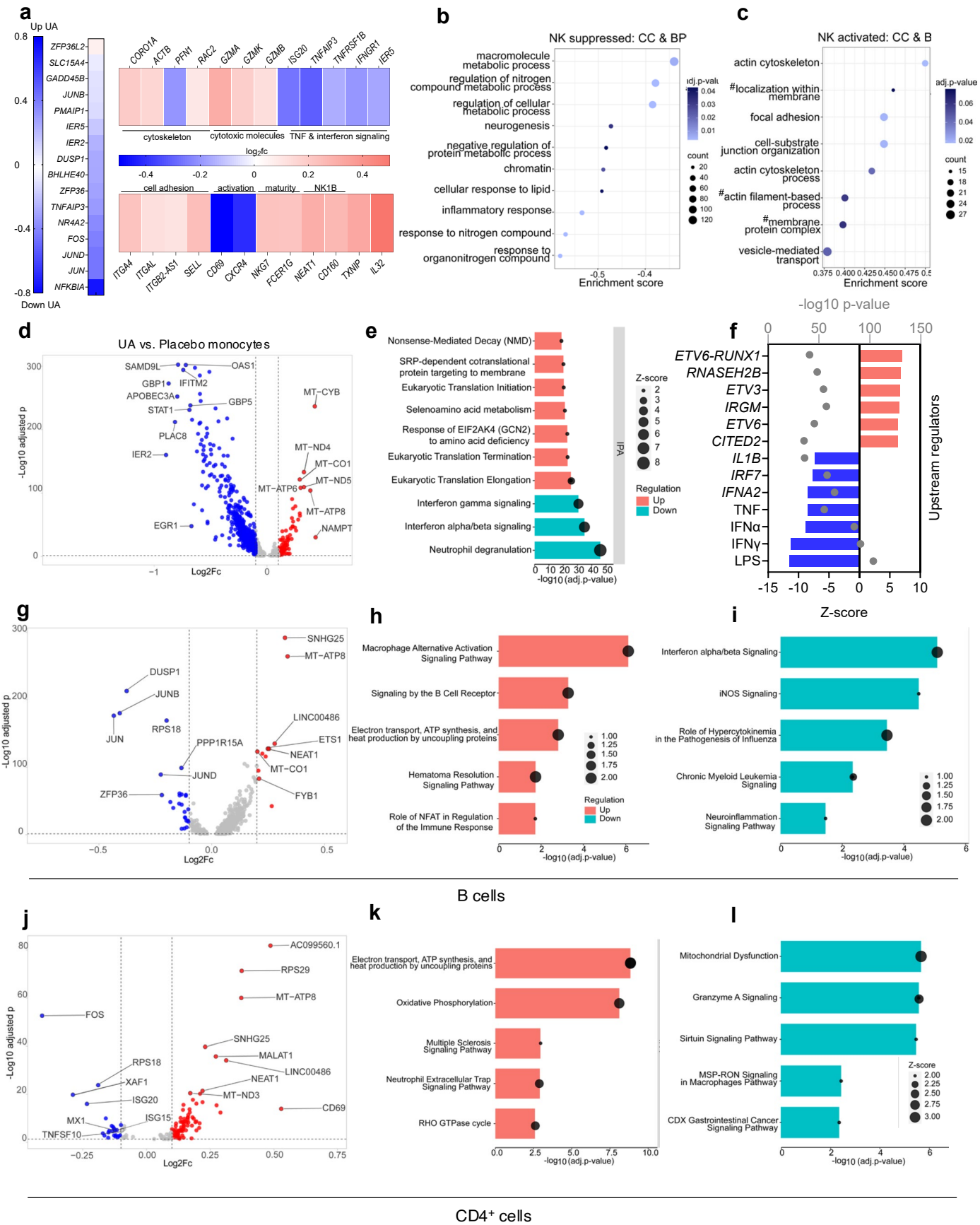

Extended Data Fig. 8 | See next page for caption.

https://doi.org/10.1038/s43587-025-00996-x

Extended Data Fig. 8 | Single cell RNA sequencing reveals UA-mediated transcriptional alterations in other immune populations. (**a**) Heatmap showing the differential expression of markers of interest among NK cells. Left shows down-regulated IEGs. The color scale is based on log2fc-scaled gene expression compared to baseline. (**b-c**) Dot plot for Gene Ontology (GO) term enrichment analysis of NK cells. Top upregulated terms and suppressed terms among BP (biological processes) and CC (cellular components) domains are shown. Ranking was performed on enrichment score. Genes with log2fc ≥ 0.1 and $p < 0.05$ were considered. (**d**) Volcano plot of differentially expressed genes within monocytes in UA treated participants vs. placebo. Red dots represent genes expressed at higher levels in monocytes from UA-treated participants, while blue dots represent genes with lower expression levels. Genes with log2fc ≥ 0.1 and $p < 0.05$ were considered significant. (**e**) Canonical pathway analysis of monocytes. Shows top 10 activated (red) and inhibited (blue) pathways in monocytes of UA-treated participants compared to the baseline measurement. Ranking was performed based on -log10 adjusted p-value. Z-scores are shown. (**f**) Upstream regulator analysis of monocytes using IPA. Top 6 predicted activated (red) and inhibited (blue) upstream regulators are shown. Ranking was performed based on Z-score. -log10 p-values are shown. (**g**) Volcano plot of differentially expressed genes within B cells in UA treated participants vs. placebo after the 28-day intervention period. Red dots represent genes expressed at higher levels in B cells from UA-treated participants, while blue dots represent genes with lower expression levels. Genes with $\log_2 fc \geq 0.1$ and $p < 0.05$ were considered significant. (**h-i**) Canonical pathway analysis of B cells. Shows top 5 activated (red; h) and inhibited (blue; i) pathways in B cells of UA-treated participants compared to the baseline measurement. Ranking was performed based on $-\log_{10}$ adjusted p-value. Z-scores are shown. (**j**) Volcano plot of differentially expressed genes within $CD4^+$ cells in UA treated participants vs. placebo after the 28-day intervention period. Red dots represent genes expressed at higher levels in CD4 cells from UA-treated participants, while blue dots represent genes with lower expression levels. Genes with $\log_2 fc \geq 0.1$ and $p < 0.05$ were considered significant. (**k-l**) Canonical pathway analysis of $CD4^+$ cells. Shows top 5 activated (red; k) and inhibited (blue; l) pathways in $CD4^+$ cells of UA-treated participants compared to the baseline measurement. Ranking was performed based on $-\log_{10}$ adjusted p-value. Z-scores are shown.

https://doi.org/10.1038/s43587-025-00996-x

Extended Data Table 1 | Biochemistry safety analysis

	UA d0	UA d28	Placebo d0	Placebo d28	p-value	baseline between groups p-value
Total cholesterol	212.5 ± 33.60	213.0 ± 33.48	201.0 ± 34.82	201.7 ± 31.40	0.9836; *n.s.*	0.2413; *n.s.*
LDL cholesterol (mg/dl) (mean ± SD)	136.6 ± 33.95	136.2 ± 30.56	127.3 ± 32.52	126.6 ± 27.76	0.9618; *n.s.*	0.3247; *n.s.*
HDL cholesterol (mg/dl) (mean ± SD)	66.06 ± 13.51	62.98 ± 17.58	62.97 ± 16.85	63.93 ± 20.65	0.0588; *n.s.*	0.4774; *n.s.*
Triglycerides (mg/dl) (mean ± SD)	154.0 ± 98.53	143.2 ± 70.34	114.7 ± 59.62	124.1 ± 78.05	0.2939; *n.s.*	0.0946; *n.s.*
Creatinine (mg/dl) (mean ± SD)	0.82 ± 0.13	0.81 ± 0.11	0.85 ± 0.18	0.85 ± 0.20	0.9868; *n.s.*	0.4280; *n.s.*
Uric acid (mg/dl) (mean ± SD)	4.86 ± 1.43	5.04 ± 1.79	4.76 ± 1.56	4.70 ± 1.45	0.1058; *n.s.*	0.7997; *n.s.*
Total serum protein (g/dl) (mean ± SD)	7.02 ± 0.38	7.06 ± 0.35	6.90 ± 0.38	6.89 ± 0.34	0.5736; *n.s.*	0.2903; *n.s.*
Albumin (g/dl) (mean ± SD)	4.54 ± 0.24	4.55 ± 0.24	4.50 ± 0.18	4.44 ± 0.20	0.3023; *n.s.*	0.5101; *n.s.*
ALT (U/l) (mean ± SD)	28.00 ± 24.02	29.44 ± 30.27	19.56 ± 8.34	19.68 ± 8.47	0.4567; *n.s.*	0.1035; *n.s.*
AST (U/l) (mean ± SD)	27.26 ± 11.51	28.04 ± 16.10	23.04 ± 4.56	23.08 ± 5.28	0.8109; *n.s.*	0.0709; *n.s.*
gGT (U/l) (mean ± SD)	24.60 ± 15.90	27.13 ± 19.19	17.64 ± 9.63	17.48 ± 9.49	0.1337; *n.s.*	0.0673; *n.s.*
AP (U/l) (mean ± SD)	75.40 ± 20.60	73.28 ± 19.22	74.48 ± 21.28	73.64 ± 22.24	0.5251; *n.s.*	0.8772; *n.s.*
Bilirubin (mg/dl) (mean ± SD)	0.53 ± 0.31	0.49 ± 0.26	0.46 ± 0.15	0.43 ± 0.15	0.7726; *n.s.*	0.3513; *n.s.*

(a) Fifty subjects (n=50) that successfully met all inclusion and exclusion criteria were randomized to either UA or placebo. The two study groups displayed similar metabolic, renal and hepatic parameters. Baseline statistics were performed within groups by paired t-testing (*n.s.*, not significant) while treatment effect was calculated using a two-sided repeated measures mixed-effects model where subjects were considered as random effects.

https://doi.org/10.1038/s43587-025-00996-x

Extended Data Table 2 | Listing of adverse events (AEs) according to groups

System Organ Class (SOC)	Lower Level Term	Urolithin A n (%) Total n=25	Placebo n (%) Total n=25
Infections and Infestations	Covid-19	1 (4%)	2 (8%)
Infections and Infestations	Upper respiratory infection	1 (4%)	1 (4%)
Respiratory, Thoracic and Mediastinal Disorders	Rhinorrhea	1 (4%)	0 (0%)
Gastrointestinal Disorders	Diarrhea	1 (4%)	0 (0%)
Gastrointestinal Disorders	Weight loss	0 (0%)	1 (4%)
Psychiatric Disorders	Depression	0 (0%)	1 (4%)

Total number of post-emergent AEs according to SOC. No life-threatening adverse events were recorded. No differences were observed between the intervention groups.

nature portfolio

Corresponding author(s): Florian Greten

Last updated by author(s): Aug 25, 2025

Reporting Summary

Nature Portfolio wishes to improve the reproducibility of the work that we publish. This form provides structure for consistency and transparency in reporting. For further information on Nature Portfolio policies, see our Editorial Policies and the Editorial Policy Checklist.

Statistics

For all statistical analyses, confirm that the following items are present in the figure legend, table legend, main text, or Methods section.

n/a	Confirmed
☐	☒ The exact sample size (*n*) for each experimental group/condition, given as a discrete number and unit of measurement
☐	☒ A statement on whether measurements were taken from distinct samples or whether the same sample was measured repeatedly
☐	☒ The statistical test(s) used AND whether they are one- or two-sided *Only common tests should be described solely by name; describe more complex techniques in the Methods section.*
☐	☒ A description of all covariates tested
☐	☒ A description of any assumptions or corrections, such as tests of normality and adjustment for multiple comparisons
☐	☒ A full description of the statistical parameters including central tendency (e.g. means) or other basic estimates (e.g. regression coefficient) AND variation (e.g. standard deviation) or associated estimates of uncertainty (e.g. confidence intervals)
☐	☒ For null hypothesis testing, the test statistic (e.g. *F*, *t*, *r*) with confidence intervals, effect sizes, degrees of freedom and *P* value noted *Give P values as exact values whenever suitable.*
☒	☐ For Bayesian analysis, information on the choice of priors and Markov chain Monte Carlo settings
☒	☐ For hierarchical and complex designs, identification of the appropriate level for tests and full reporting of outcomes
☒	☐ Estimates of effect sizes (e.g. Cohen's *d*, Pearson's *r*), indicating how they were calculated

Our web collection on statistics for biologists contains articles on many of the points above.

Software and code

Policy information about availability of computer code

Data collection	SecuTrial; https://www.secutrial.com/
Data analysis	GraphPad Prism, Version 10; SAS® Version 9.4 with SAS Enterprise Guide Version 8.3

For manuscripts utilizing custom algorithms or software that are central to the research but not yet described in published literature, software must be made available to editors and reviewers. We strongly encourage code deposition in a community repository (e.g. GitHub). See the Nature Portfolio guidelines for submitting code & software for further information.

Data

Policy information about availability of data

All manuscripts must include a data availability statement. This statement should provide the following information, where applicable:

- Accession codes, unique identifiers, or web links for publicly available datasets
- A description of any restrictions on data availability
- For clinical datasets or third party data, please ensure that the statement adheres to our policy

scRNAseq data of participant PBMCs are publicly available in the NCBI Sequence Read Archive (SRA) under BioProject accession number PRJNA1169651.
The minimum de-identified dataset to generate the graphs that support the findings are available from the corresponding author.

Research involving human participants, their data, or biological material

Policy information about studies with human participants or human data. See also policy information about sex, gender (identity/presentation), and sexual orientation and race, ethnicity and racism.

Reporting on sex and gender	Intervention groups were randomised according to sex, hence both intervention groups included the same sex distribution. which is displayed in the Extended Data Set. Due to sample size limitations, no specific gender-based analysis were performed.
Reporting on race, ethnicity, or other socially relevant groupings	No specific measurements were taken or intended to include or exclude participants of a certain ethnicity. Participants were enrolled based on inclusion and exclusion criteria, which did not specifically include ethnicity. Definition of ethnicity was self-reported by the participants and stored in the eCRF. All participants identified as caucasian.
Population characteristics	Populations characteristics are displayed in the Extended Data set.
Recruitment	Participants were recruited from health care workers and scientific staff from the Georg-Speyer-Haus and University Hospital Frankfurt, respectively. Additional participants were recruited via social media advertisement previously approved by the institutional review board. Participants were recruited from 03/2023 to 12/2023. The study only inlcuded participants that met all inclusion and exclusion criteria (healthy, aged adults), and the results may not generalize to other diseases or age groups.
Ethics oversight	Our study was approved and monitored by the local IRB of the University of Frankfurt, Germany (Ethikkommission des Fachbereichs Medizin der Goethe-Universität, approval number 2022-745_2)

Note that full information on the approval of the study protocol must also be provided in the manuscript.

Field-specific reporting

Please select the one below that is the best fit for your research. If you are not sure, read the appropriate sections before making your selection.

☒ Life sciences ☐ Behavioural & social sciences ☐ Ecological, evolutionary & environmental sciences

For a reference copy of the document with all sections, see nature.com/documents/nr-reporting-summary-flat.pdf

Life sciences study design

All studies must disclose on these points even when the disclosure is negative.

Sample size	Sample size estimates were based on statistical simulations by Jacques et al (doi: 10.1096/fj.201901997RR) where a comprehensive literature review was performed to assess range of effect size for 80% power when oxidative function of muscle cells was studied. According to these statistical simulations, 24 participants are considered sufficient for interventions with an expected 11% effect size. Likewise, the sample size chosen (n=50) is comparable to a similar study in the literature (doi: 10.1172/JCI138538) that focused on immune health and mitochondrial function.
Data exclusions	No data was excluded for the primary endpoint analysis, rendering n=25 per group. For cytokine measurements, samples that did not provide any measurable levels were excluded from analysis (1-2 measurements per group), which is specified in the paper.
Replication	For each assay, each participants was only measured once; hence all replicates correspond to biological replicates, not technical replicates. These biological replicates ranged from n=12-25. Only statistically significant findings were used to draw conclusions. This marks a proof-of-concept phase I study which has addressed the primary and secondary aims. Thus, future trials are needed to confirm these findings and its potential translation to other cohorts and diseases.
Randomization	Upon study participant inclusion and informed consent, randomization was performed double-blind at the study site, using the eCRFs (Secutrial) web-based, in-built randomization platform. A static stratified block randomization algorithm was used, randomizing participants according to age, gender and BMI. For this block-based randomization strategy, a block size of four was used. All participants received the allocated intervention.
Blinding	The investigational product was blinded into a study code by an unblinded person at the sponsor site, who was not involved in trial design, data collection, analysis or interpretation of the data. Data collection and analysis was performed blinded. Unblinding was performed after analysis of primary and secondary endpoints.

Reporting for specific materials, systems and methods

We require information from authors about some types of materials, experimental systems and methods used in many studies. Here, indicate whether each material, system or method listed is relevant to your study. If you are not sure if a list item applies to your research, read the appropriate section before selecting a response.

Materials & experimental systems

n/a	Involved in the study
☐	☒ Antibodies
☒	☐ Eukaryotic cell lines
☒	☐ Palaeontology and archaeology
☒	☐ Animals and other organisms
☐	☒ Clinical data
☒	☐ Dual use research of concern
☒	☐ Plants

Methods

n/a	Involved in the study
☒	☐ ChIP-seq
☐	☒ Flow cytometry
☒	☐ MRI-based neuroimaging

Antibodies

Antibodies used

Detailed information regarding antibodies used including clone, vendors and catalogue numbers are provided in the Methods section and the Supplementary Information.

Validation

The commercially-available antibodies are field standards and have been validated by the respective vendor. A list of antibodies for the staining panels has been provided in the Supplementary Information. The antibody mixes for the broad immune profiling were concomittantly tested on a "standard" sample (healthy, frozen PBMC) with known immune cell distirbution to ensure validity of the staining and gating strategy. A gating strategy showing positive/negative separation is provided in the Supplementary Information.

Clinical data

Policy information about clinical studies

All manuscripts should comply with the ICMJE guidelines for publication of clinical research and a completed CONSORT checklist must be included with all submissions.

Clinical trial registration

The study was registered prior to the enrollment of the first participant on clinicaltrials.gov:NCT05735886.

Study protocol

The study protocol is made available with the paper.

Data collection

The data was collected at Georg-Speyer-Haus, Frankfurt and University Hospital, Frankfurt from 2023-2024. Informed consent was obtained from all participants.
Participants were healthy volunteers; therefore we cannot exclude self-selection bias and inclusion of participants that inherently aim to live a healthier lifestyle.

Outcomes

Primary outcomes:
1)Change in percentages of CD3+ T-cell immune cell population
In particular, number of CD8+ T memory stem cells and naïve-like T cells (flow cytometry)
[Time Frame: 28 days]
2) Change in Mitochondrial activity in CD3+ T-cells
Mitochondrial function evaluated via SCENITH metabolic profiling (flow cytometry)
[Time Frame: 28 days]

Secondary outcomes:
1) Change in pro and anti-inflammatory cytokine levels (IL-6, TNF-a, IL1-B, IL-10) in plasma measured by bead-based flow cytometry
[Time Frame: 28 days]
1. Change in percentages of other immune cell populations (B cells, NK cells, Macrophages, DCs etc.) via flow cytometry
[Time Frame: 28 days]
2. Change in Mitochondrial content on CD3 T-cell populations via Mitotracker staining using flow cytometry
[Time Frame: 28 days]
3. Change in gene-expression: single cell analysis of CD3+ T-cells
[Time Frame: 28 days]
4. Change in PBMC's immune function assessment (cytokine secretion, bacterial engulfment) via flow cytometry
[Time Frame: 28 days]
5. Change in Lipid profile
[Time Frame: 28 days]
6. Number of adverse events
[Time Frame: 28 days]

Plants

Seed stocks — *Report on the source of all seed stocks or other plant material used. If applicable, state the seed stock centre and catalogue number. If plant specimens were collected from the field, describe the collection location, date and sampling procedures.*

Novel plant genotypes — *Describe the methods by which all novel plant genotypes were produced. This includes those generated by transgenic approaches, gene editing, chemical/radiation-based mutagenesis and hybridization. For transgenic lines, describe the transformation method, the number of independent lines analyzed and the generation upon which experiments were performed. For gene-edited lines, describe the editor used, the endogenous sequence targeted for editing, the targeting guide RNA sequence (if applicable) and how the editor was applied.*

Authentication — *Describe any authentication procedures for each seed stock used or novel genotype generated. Describe any experiments used to assess the effect of a mutation and, where applicable, how potential secondary effects (e.g. second site T-DNA insertions, mosiacism, off-target gene editing) were examined.*

Flow Cytometry

Plots

Confirm that:

☒ The axis labels state the marker and fluorochrome used (e.g. CD4-FITC).

☒ The axis scales are clearly visible. Include numbers along axes only for bottom left plot of group (a 'group' is an analysis of identical markers).

☒ All plots are contour plots with outliers or pseudocolor plots.

☒ A numerical value for number of cells or percentage (with statistics) is provided.

Methodology

Sample preparation — Spectral flow cytometry to broadly analyze immune composition was performed on PBMCs from 25 UA and 25 placebo individuals from our cohort. Flow cytometry staining was performed in three batches to minimize to batch-related effects. PBMC were thawed and allowed to recover for 3 hours in uncoated cell culture dishes. All samples for any particular donor series were thawed together. Cells were stained with the panel shown in the Supplementary Figures.

Instrument — Data was acquired by Cytek Aurora, generating FCS files.

Software — FCS files were exported into FlowJo (BD, Version 10) for further analysis

Cell population abundance — Alive abCD8+ cells ranged from 30,000 - >200,000.

Gating strategy — Cells were identified by a initial SSC/FSC plot, followed by identification of single cells via FSC-H/FSC-A. Next, alive CD45+ cells were gated by the use of an anti-CD45 antibody and viability dye. A representative gating strategy depicting these steps is provided in the Supplementary Information.

☒ Tick this box to confirm that a figure exemplifying the gating strategy is provided in the Supplementary Information.